Article

RNA-triggered cell killing with CRISPR–Cas12a2

https://doi.org/10.1038/s41586-026-10466-y

Received: 11 March 2025

Accepted: 26 March 2026

Published online: 06 May 2026

Open access

Check for updates

Paul Scholz[1,10]✉, Jared Thompson[2,10], Kadin T. Crosby[3,10], Torsten Fauth[1], Nathan M. Krah[2,4], Grant Schlauderaff[2], Robin Back[1], Zachary A. Berkheimer[2], Alivia Jolley[2], Dirk Sombroek[1], Rebekka Medert[1], Christian Zurek[5], Oleg Dmytrenko[6], Emily Wilson[7], Friso T. Schut[6], Jared Rutter[2,8], Xiaoyang Zhang[7], Michael Krohn[1], Ryan N. Jackson[3]✉, Chase L. Beisel[6,9]✉ & Yang Liu[2]✉

Selectively eradicating target cells on the basis of their genetic or transcriptional identity remains important in basic research, medicine, biotechnology and agriculture[1–3]. For applications involving bacteria, CRISPR nucleases offer promising options due to their ability to enact RNA-guided counterselection[4–7]; however, using these same nucleases for counterselection in eukaryotes has proven much more restrictive[8–14]. Here we show that Cas12a2, a recently discovered type V CRISPR nuclease, exhibits RNA-triggered DNA shredding[15,16], and enables programmable and sequence-specific elimination of yeast and human cells expressing a target transcript. Triggering Cas12a2 elicits rampant double-stranded DNA breaks *in trans*, leading to cell death. Cell killing can be activated by a wide range of target transcripts, with no observed off-target activation. Leveraging this approach, we selectively eliminate cells that harbour human papillomavirus, cells that failed to undergo gene editing, or cells that encode a prevalent oncogenic point mutation in *KRAS*. These findings expand the CRISPR toolbox to allow the selective elimination of eukaryotic cells on the basis of their transcriptional profile.

Selectively eliminating cells, tissues and organisms on the basis of their genetic or physiological identity has been a mainstay of the life sciences, whether for precisely removing diseased cells, shaping cellular communities, or eradicating contaminants or pathogens[1–3]. Common molecular and cell-based interventions, such as small-molecule inhibitors, toxins, antibodies, lytic viruses or programmed immune cells, eliminate cells through specific proteins or survival pathways[17–20]; however, these methods cannot be tailored to arbitrary genetic or transcriptional states as well as difficult-to-drug scenarios such as mutations in non-coding sequences or complex aetiologies. A cell-killing approach triggered directly by the specific recognition of prescribed DNA or RNA sequences could greatly broaden the range of targetable conditions, creating new means to counterselect against specific cells in a variety of situations and applications.

CRISPR nucleases—RNA-guided effector proteins of CRISPR–Cas immune systems in bacteria and archaea[21]—have various biochemical activities triggered by recognizing targeted DNA or RNA; such activities could be harnessed to selectively eliminate cells on the basis of their genetic or transcriptional state[22–25]. In bacteria, CRISPR nucleases potently eliminate cells containing a target sequence via different mechanisms; for example, Cas9 and Cas12a introduce targeted double-stranded DNA (dsDNA) breaks that are poorly repaired[4,5], or Cas13a collaterally cleaves RNA driving cell dormancy[6,7]. However, these activities are largely ineffective for programmed cell elimination in eukaryotic cells. Instead of resulting in cell death, dsDNA breaks by Cas9 or Cas12a are efficiently repaired through homology-directed repair (HDR) or non-homologous end joining (NHEJ)[26–28]. Only when targeted cleavage occurs throughout the genome, such as by targeting highly repetitive elements, can these nucleases induce cell death[12–14]. Separately, activating Cas13 in eukaryotic cells usually leads to specific degradation of the target transcript[10]. When indiscriminate RNA degradation has been observed, activated Cas13 fails to drive robust cell dormancy or death[8–11]. Thus, CRISPR-based approaches that broadly enable selective cell elimination in bacteria remain elusive in eukaryotes.

We recently reported a clade of RNA-guided CRISPR nucleases called Cas12a2 that, upon specifically base pairing with complementary RNA, unleashes indiscriminate dsDNase activity that drives an SOS DNA damage response and cell dormancy in bacteria[15,16]. However, the effect of Cas12a2's RNA-triggered indiscriminate dsDNase activity remained unexplored in eukaryotes. We thus asked how Cas12a2 affects eukaryotic cells when unleashed by specific recognition of a transcript and whether these nucleases can be used for RNA-triggered programmable cell elimination.

[1]Akribion Therapeutics GmbH, Zwingenberg, Germany. [2]Department of Biochemistry, University of Utah School of Medicine, Salt Lake City, UT, USA. [3]Department of Chemistry and Biochemistry, Utah State University, Logan, UT, USA. [4]Department of Internal Medicine, University of Utah, Salt Lake City, UT, USA. [5]BRAIN Biotech AG, Zwingenberg, Germany. [6]Helmholtz Institute for RNA-based Infection Research (HIRI), Helmholtz Centre for Infection Research (HZI), Würzburg, Germany. [7]Department of Oncological Sciences, Huntsman Cancer Institute, University of Utah, Salt Lake City, UT, USA. [8]Howard Hughes Medical Institute, University of Utah School of Medicine, Salt Lake City, UT, USA. [9]Medical Faculty, University of Würzburg, Würzburg, Germany. [10]These authors contributed equally: Paul Scholz, Jared Thompson, Kadin T. Crosby. ✉e-mail: paul.scholz@akribion-therapeutics.com; ryan.jackson@usu.edu; chase.beisel@helmholtz-hiri.de; yang.liu@biochem.utah.edu

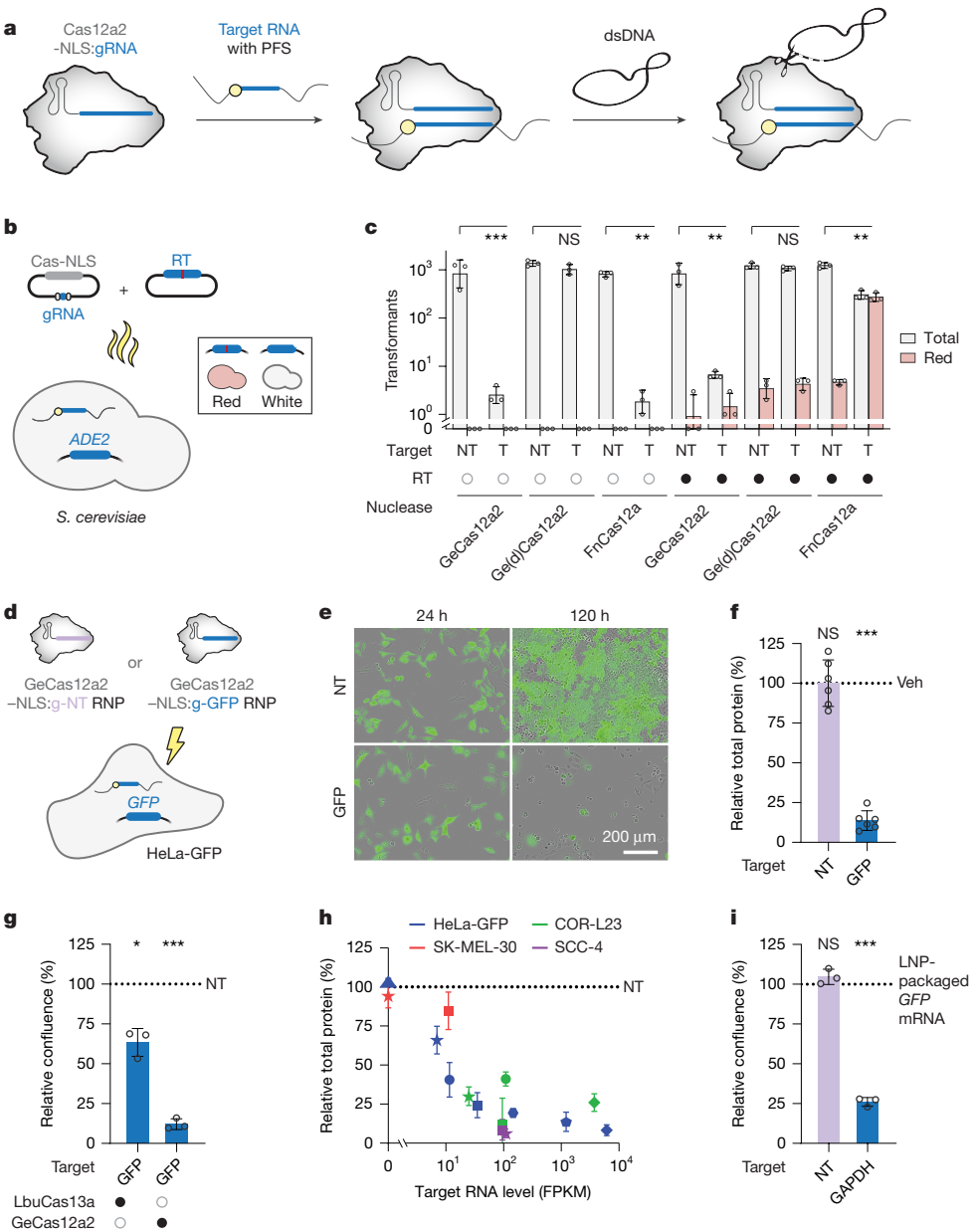


Fig. 1 | RNA-triggered Cas12a2 eliminates yeast and mammalian cells expressing a target RNA sequence. a, Properties of Cas12a2 nucleases. **b**, Interrogating the effect of Cas12a2 in *S. cerevisiae*. gRNAs direct GeCas12a2 or FnCas12a to the *ADE2* transcript or encoding DNA sequence. A DNA repair template disrupts the target site and *ADE2* expression, resulting in red pigment accumulation. **c**, Yeast colony counts and fraction that are red colonies. RT, repair template; T, targeting; NT, non-targeting. **d**, Interrogating the effect of RNA-triggered Cas12a2 in human cells. **e**, Overlaid phase contrast and GFP fluorescence microscopy images following electroporation with GeCas12a2 RNPs bearing an NT or *GFP*-targeting guide (GFP) in HeLa-GFP cells. **f**, Cell quantification by sulforhodamine B staining (SRB) following electroporation with GeCas12a2 RNPs against the indicated targets in HeLa-GFP cells. Dotted line, normalized to vehicle (Veh). **g**, Cell quantification by phase contrast imaging (confluence) following electroporation with GeCas12a2 or LbuCas13a RNPs against the *GFP* target in HeLa-GFP cells, normalized to non-target. **h**, Cell quantification by SRB relative to target RNA FPKM levels following electroporation of on-target GeCas12a2 RNPs across four different cell lines, normalized to non-target. Target transcripts: circle, *KRAS-PAN*; star, *EGFR*; square, *TP53*; triangle, *CD8A*; hexagon, *MALAT1*; pentagon, *GFP*; diamond, *GAPDH*. Shapes and error bars represent the mean and s.d. of biological replicates ($n = 3, 4, 6$ or 7). **i**, Cell quantification by confluence imaging following co-delivery of LNP-packaged GeCas12a2 and gRNAs against the indicated targets in HEK293T cells, normalized to an LNP-packaged *GFP* mRNA control. Circles in **c**, **f**, **g** and **i** represent biological replicates ($n = 3$ or 6); bars and error bars represent the mean and s.d. Two-tailed unpaired *t*-test with Welch's correction was performed; NS, $P > 0.05$; $^{*}P < 0.05$; $^{**}P < 0.01$; $^{***}P < 0.001$.

Cas12a2 eliminates yeast cells

To explore the effect of triggering Cas12a2 nucleases in eukaryotic cells, we used two closely related variants of Cas12a2: one from *Sulfuricurvum* sp. PC08-66 (SuCas12a2), and another derived from a metagenomic sample (GeCas12a2). The enzymes share 89% identity (Extended Data Fig. 1) and have similar biochemical properties, including recognition of RNA targets upstream of an adenine-rich protospacer-flanking sequence (PFS) and subsequent collateral cleavage of RNA, single-stranded DNA and dsDNA (Fig. 1a and Supplementary Fig. 2, Extended Data Figs. 1 and 2, and Supplementary Table 1), lending themselves to the same strategy for guide RNA (gRNA) design (Extended Data Fig. 3).

We first tested Cas12a2 activity in the yeast *Saccharomyces cerevisiae* as a simple model for the elimination of eukaryotic cells by

transforming a plasmid expressing GeCas12a2 fused to nuclear localization signals (NLSs) and a designed gRNA targeting the transcript of the non-essential gene *ADE2* (Fig. 1b). Here, an included DNA repair template enabled local HDR that inactivates *ADE2*, resulting in formation of a red pigment[29], and disrupted the nuclease target site, similar to an insertion or deletion with traditional DNA-cutting Cas nucleases. Under targeting conditions, GeCas12a2 reduced transformants by 134-fold versus non-targeting conditions, regardless of whether a repair template was present (Fig. 1c). The nuclease activity of GeCas12a2 was necessary, as a catalytically dead RuvC mutant (Ge(d)Cas12a2) failed to reduce transformants. Furthermore, there was no measurable increase in red transformants with active GeCas12a2, ruling out escape through HDR. By contrast, the DNA-cutting FnCas12a reduced the transformants by only fourfold with the repair template, with 90% of the transformants expressing red pigment, indicative of HDR. Thus, Cas12a2 drives efficient target-dependent elimination of yeast cells despite the opportunity for localized DNA repair provided by donor DNA, unlike traditional DNA-cutting nucleases.

Cas12a2 eliminates human cells

We next examined the effect of triggering Cas12a2 in human cells, which can repair double-strand breaks through NHEJ and HDR[30,31]. As a first test, we electroporated a GeCas12a2–gRNA ribonucleoprotein complex (RNP)—which targets the green fluorescent protein (*GFP*) transcript—into a HeLa cell line stably expressing *GFP* at high levels (Supplementary Table 2) and monitored cell proliferation using fluorescence microscopy (Fig. 1d). We used a truncated 21-nt guide previously shown to have the same targeting activity as a 24-nt guide[15]. HeLa-GFP cells electroporated with a *GFP*-targeting RNP failed to proliferate and even noticeably decreased in number over time. By contrast, a non-targeting RNP with a guide complementary to the *AspLigD* transcript from *Aspergillus* (absent in the human genome) or a catalytically dead *GFP*-targeting RNP resulted in typical cell growth, reaching confluence in a few days (Fig. 1e and Supplementary Fig. 3). Quantifying total protein levels of adhered cells after 5 days of culturing resulted in 86% cell depletion compared with the non-targeting RNP control (Fig. 1f). Electroporation of an SuCas12a2 RNP lacking an NLS similarly depleted HEK293-GFP cells when targeting *GFP* transcript (Supplementary Fig. 4). LbuCas13a, which has been shown to also drive cell depletion when activated in human cells[32], led to only modest depletion (37%) when targeting the same site in the *GFP* transcript, despite the transcript activating LbuCas13a in vitro (Fig. 1g and Extended Data Fig. 4). These findings show that Cas12a2 can drive elimination of human cells upon specific recognition of transcripts.

Building on this initial demonstration, we targeted six endogenous transcripts across four cell lines derived from melanoma, lung, and head and neck cancers (Fig. 1h and Supplementary Table 2), with transcript levels varying from undetectable to highly expressed and differing between cell lines. GeCas12a2 yielded cell depletion compared with the non-targeting *AspLigD* control across all cell types, even when targeting poorly expressed transcripts. Importantly, GeCas12a2 also depleted PC3 cells that have longer doubling times and show tolerance to the DNA damage-inducing agent etoposide (Supplementary Fig. 5). Some transcripts with poor or undetectable expression did not elicit cell depletion, consistent with a dependency on transcript abundance. Cell depletion was also dependent on the concentration of delivered RNP, with lower concentrations leading to less depletion and GeCas12a2 outperforming SuCas12a2 with the same NLSs at lower RNP concentrations (Supplementary Fig. 6). GeCas12a2 could also drive target-dependent cell depletion when delivered as an mRNA and gRNA packaged in lipid nanoparticles (LNPs) (Fig. 1i). Overall, these results show that Cas12a2 can be programmed to drive specific cell depletion even for poorly expressed transcripts in multiple cell types and with different delivery modalities.

Cas12a2 induces lethal dsDNA breaks

Cas12a2 eliminated yeast and human cells in the presence of a specific target transcript, yet it was unclear whether the dsDNase activity of Cas12a2 drove cell death. After confirming that RNA-triggered GeCas12a2 could degrade purified chromosomal DNA (Fig. 2a), we probed the intracellular effect of triggering GeCas12a2 in HeLa-GFP cells one day after RNP delivery by quantifying the number of dsDNA breaks formed in cells via immunofluorescence staining for 53BP1—an endogenous repair protein that forms foci at double-strand breaks[33] (Fig. 2b,c). GeCas12a2 targeting either *GFP* or *GAPDH* transcripts induced at least 5.2-fold more 53BP1 foci than non-targeting and vehicle-only conditions. Notably, the number of dsDNA break foci associated with RNA-triggered Cas12a2 is comparable with levels observed in cells treated with the widely used DNA-damaging anti-cancer drugs cisplatin and etoposide[34,35]. Although these drugs cause indiscriminate DNA damage in healthy and cancer cells, Cas12a2 only induces DNA damage above background levels when cells express the target transcript.

DNA damage—and particularly severe amounts of dsDNA breaks—can lead to cell cycle arrest and cell death[36]. To characterize the effect of GeCas12a2-induced DNA damage, we performed cell cycle analysis on the basis of cellular DNA content following electroporation of *GFP*-targeting RNPs into HeLa-GFP cells. Our analysis revealed a 2.5-fold reduction in the G1 cell population and the emergence of cells with irregular DNA copy numbers in the sub-G1 and >4N regions—hallmarks of mitotic catastrophe[37] and apoptosis[38] (Fig. 2d,e). We further found that treatment with the *GFP*-targeting GeCas12a2 RNP led to around 40% of cells staining with fluorescent annexin V protein or a substrate of activated caspase-3/7 after two days, suggesting induction of apoptosis (Fig. 2f,g). At the same time, the DNA-binding dye 4′,6-diamidino-2-phenylindole (DAPI) exclusively stained about 20% of the cells (Supplementary Fig. 7)—a potential indicator of necrosis. By contrast, RNA-sequencing (RNA-seq) analysis revealed upregulation of specific inflammatory gene sets at levels comparable with those observed with nigericin—a potent activator for NLRP3-dependent inflammasomes and lytic cell death pathways[39] (Fig. 2h and Supplementary Fig. 8). Electroporated SuCas12a2 RNPs lacking an NLS similarly caused elevated 53BP1 foci, characteristic shifts in the cell cycle distribution, and increased annexin V affinity and caspase-3/7 activity under targeting conditions (Supplementary Fig. 9). We therefore conclude that RNA-triggered Cas12a2 nucleases eliminate human HeLa-GFP cells through extensive DNA damage followed principally by apoptosis but also other cell death pathways.

Minimal off-target activation by Cas12a2

Recognition of a complementary transcript flanked by a PFS activates Cas12a2, leading to extensive DNA damage and cell death. Depending on the propensity of Cas12a2 to tolerate mismatches or non-canonical PFSs, we reasoned that the nuclease may inadvertently recognize non-target transcripts with sequence similarity to the intended target, driving cell killing in the absence of the target transcript. We call such an event off-target activation. As activation by a target or off-target RNA alike would lead to the same cell death outcome, identifying potential off-target transcripts by Cas12a2 requires a distinct approach compared to existing strategies commonly used with Cas nucleases[40–42].

We reasoned that the most straightforward way to probe off-target activation of GeCas12a2 was to assess cells transfected with RNPs containing guides that target transcripts that are naturally absent in human cells. Neither non-targeting nor *GFP*-targeting RNPs depleted HeLa cells lacking *GFP* (Fig. 3a). Furthermore, compared with the vehicle-only control, neither RNP—on the basis of 53BP1 foci formation—drove a measurable increase in dsDNA breaks (Fig. 3b). Separately, assessing

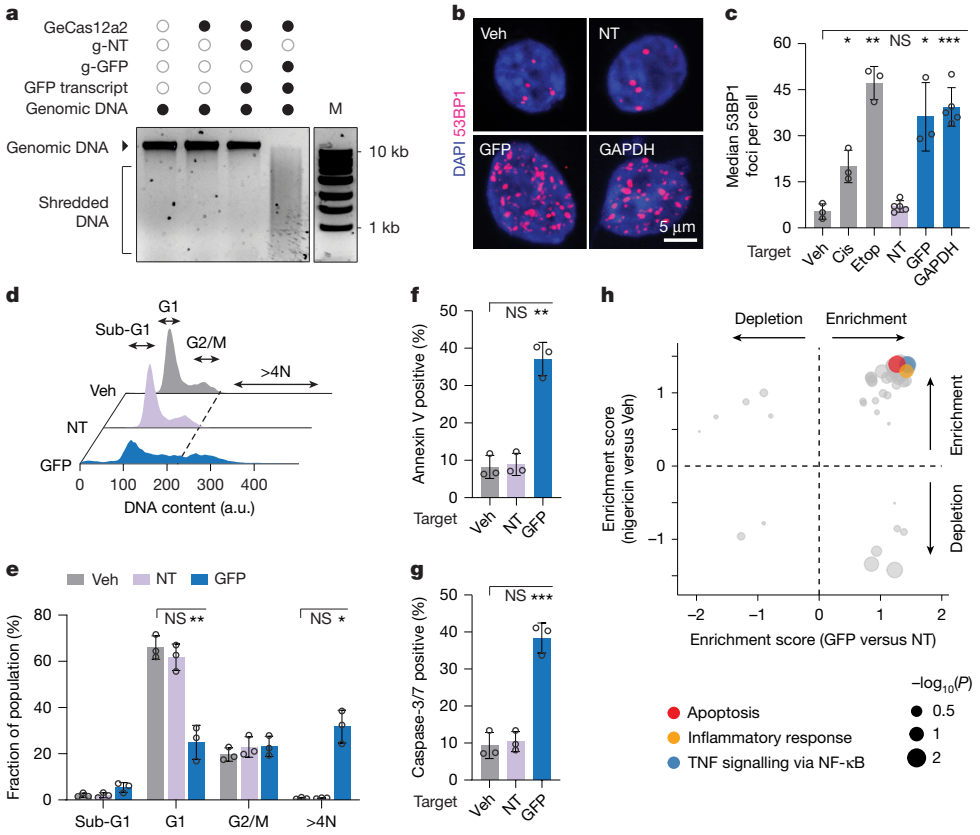


Fig. 2 | RNA-triggered Cas12a2 induces extensive dsDNA breaks followed by cell death. a, Cleavage of purified HeLa-GFP genomic DNA exposed to GeCas12a2 under activating and non-activating conditions in vitro. Representative of three independent replicates. **b**, Representative confocal images of endogenous 53BP1 foci (magenta) formed at dsDNA breaks in the nuclei (DAPI, blue) following electroporation with GeCas12a2 RNPs against the indicated targets in HeLa-GFP cells. **c**, Quantification of median 53BP1 foci per cell 24 h after treatment with 1 µM of cisplatin (Cis) or etoposide (Etop) or with GeCas12a2 RNPs against the indicated targets in HeLa-GFP cells. In total, 250–450 cells were analysed per condition. Veh, vehicle only. **d**, Quantification of DNA content per cell following electroporation with GeCas12a2 RNPs against the indicated targets in HeLa-GFP cells after 48 h. Histogram traces show distributions of cellular DNA content determined by DAPI staining for one representative biological replicate ($n = 3$). About 10,000 total cells were analysed per replicate. **e**, Percentage of population in distinct cell cycle stages based on the gating shown in **d**. **f**,**g**, Percentage of cells positive for annexin V staining (**f**) or caspase 3/7 activity (**g**) 48 h following electroporation with GeCas12a2 against the indicated targets in HeLa-GFP cells. **h**, Enrichment scores from a gene set enrichment analysis (GSEA) for cells treated with nigericin or GeCas12a2 RNPs targeting the *GFP* transcript compared with negative controls in HeLa-GFP cells. Hallmark gene sets for apoptosis and key inflammatory pathways are highlighted. Enrichment score and significance for each pathway was determined by two-tailed permutation test with Benjamini–Hochberg adjustment for multiple comparisons from the average of three biological replicates, implemented in fGSEA. Circles in **c**,**e**–**g** represent biological replicates ($n = 3$, 4 or 5), bars and error bars represent the mean and s.d. Two-tailed unpaired *t*-test with Welch's correction was performed; NS, $P > 0.05$; $^{*}P < 0.05$; $^{**}P < 0.01$; $^{***}P < 0.001$.

the NHEJ-mediated integration of a co-delivered dsDNA barcode in the same cells[43] (Fig. 3c and Supplementary Table 3) by quantitative polymerase chain reaction (qPCR) yielded no measurable increase in integrated barcodes for either non-targeting or *GFP*-targeting RNPs (Fig. 3d). By contrast, a GeCas12a2 RNP targeting the endogenous *GAPDH* transcript yielded significant dsDNA barcode integration, consistent with indiscriminate dsDNA breaks caused by Cas12a2 on-target activity. We therefore found no evidence of either guide inducing off-target activation in these cells.

A separate means of evaluating off-target activation, particularly when the target transcript cannot be readily removed, is to investigate whether any genomically encoded transcripts could activate collateral cleavage by an RNP in vitro. Potential activating RNAs could originate from either strand of DNA or from RNA splicing, so we conservatively predicted genomic and copy DNA (cDNA) sites with extensive complementarity to either a *GFP*-targeting or non-targeting guide (Methods). No sites were identified with a single mismatch, although we identified off-target candidates with two (4 for NT, 1 for *GFP*) or three (37 for NT, 10 for *GFP*) mismatches (Supplementary Tables 4 and 5). We tested the two-mismatch candidates, along with selected three-mismatch candidates flanked by a probable PFS and a four-mismatch candidate carrying the canonical PFS (Fig. 3e). Among these, only one putative off-target yielded modest activation of GeCas12a2 in vitro (Fig. 3f), for which the associated transcript is poorly expressed in HeLa-GFP cells (1 FPKM (fragments per kilobase of exon per million fragments mapped)) and HEK293-GFP cells (2.5 FPKM) (refer to the Methods for a definition of FPKM; Supplementary Table 2).

Given that a mismatched RNA sequence activated Cas12a2 in vitro, we systematically assessed mismatch tolerance in cells. Using the *GFP* target, we tested paired mismatches across the length of a 21-nt guide (Fig. 3g), reflecting the smallest number of mismatches predicted for off-target activation (Supplementary Tables 4–6). All tested mismatches resulted in no measurable depletion of HeLa-GFP cells (Fig. 3h). As a further readout of Cas12a2 off-target activation, we performed RNA-seq analysis on HeLa-GFP cells treated with a non-targeting guide as well as a *GFP*-targeting guide as a positive control. The non-target guide showed no differential gene expression compared to the vehicle-only control despite potential off-targets, whereas the on-target *GFP* guide triggered differential expression of over 800 genes (Fig. 3i). Thus, under our experimental conditions and tested gRNAs, Cas12a2 activity was

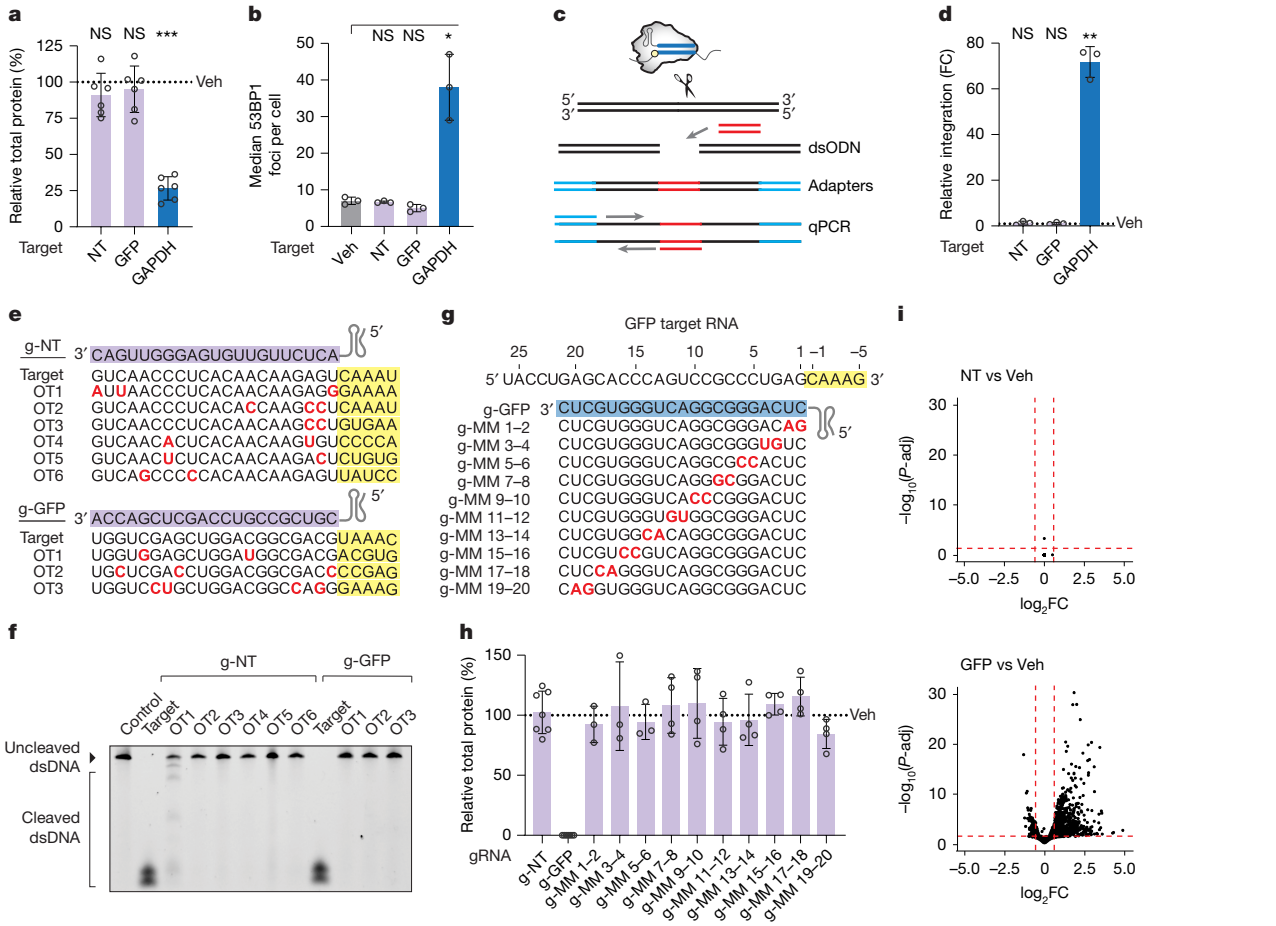


Fig. 3 | Cas12a2 has limited off-target activation in human cells. a, Cell quantification by SRB following electroporation with GeCas12a2 RNPs against the indicated targets in HeLa cells, normalized to vehicle. **b**, Quantification of median 53BP1 foci per cell 24 h following electroporation with GeCas12a2 RNPs against the indicated targets in HeLa cells, normalized to vehicle. In total, 175–275 cells were analysed per condition. **c**, Investigating off-target dsDNA breaks via integration of a double-strand oligodeoxynucleotide (dsODN) barcode detected by qPCR. **d**, Quantification of dsODN integration by qPCR following electroporation with GeCas12a2 against the indicated targets in HeLa cells, normalized to vehicle. FC, fold change. **e**, Examining potential off-target RNA sequences for non-targeting and *GFP*-transcript-targeting gRNAs. Mismatches are indicated in bold red, whereas PFS are highlighted yellow. **f**, dsDNA cleavage assay to assess GeCas12a2 activation potential in vitro with off-target (OT) transcripts identified in **e**. Representative of three independent replicates. **g**, Interrogating mismatch tolerance of Cas12a2 with double-mismatch gRNAs against the *GFP* target. Mismatches bolded in red, PFS highlighted with yellow. **h**, Cell quantification by SRB following electroporation with GeCas12a2 RNPs and mismatched gRNAs against the *GFP* target in HeLa-GFP cells, normalized to vehicle. **i**, Volcano plots of all differentially expressed transcripts 48 h following electroporation with GeCas12a2 against the indicated targets compared to vehicle in HeLa-GFP cells. Expression values were determined by two-tailed Wald tests with Benjamini–Hochberg adjustments for multiple comparisons from the average of three biological replicates, implemented in DESeq2. Circles in **a**,**b**,**d** and **h** represent biological replicates ($n = 3, 4, 6$ or 7), bars and error bars represent the mean and s.d. Two-tailed unpaired *t*-test with Welch's correction was performed; NS, $P > 0.05$; $^{*}P < 0.05$; $^{**}P < 0.01$; $^{***}P < 0.001$.

sensitive to mismatches and did not yield measurable off-target activation in human cells.

Cas12a2 eliminates virally infected cells

Given Cas12a2's ability to eliminate human cells on the basis of a selected target transcript, we envisioned a versatile approach that could counterselect against undesired cells while sparing desired cells on the basis of distinct transcriptional profiles (Fig. 4a). We sought to explore the potential of this approach through three general scenarios: eliminating cells chronically infected with viruses while sparing uninfected cells, eliminating unedited cells while enriching edited cells, and selectively eliminating cancer cells with established somatic point mutations.

For the first scenario, we targeted cells harbouring high-risk variants of human papillomavirus (HPV). This scenario is arguably the most straightforward for selective elimination, as the viral transcripts are absent in the human transcriptome and offer numerous potential target sites specific to the virus. We therefore designed gRNAs targeting the moderately expressed HPV transcripts encoding E6 or E7 oncoproteins (Fig. 4b, Supplementary Tables 6 and 7), which led to robust activation of GeCas12a2 in vitro in the presence of the corresponding transcript (Extended Data Fig. 5). Electroporating *E6*- or *E7*-targeting GeCas12a2 RNPs into HeLa-GFP cells resulted in 94% cell reduction for both compared with the non-targeting control (Fig. 4c). By contrast, applying the same RNPs to HEK293-GFP cells, which lack HPV, showed no significant cell depletion. Furthermore, introducing five different single-base mutations in the guide resulted in a complete loss of cell depletion for all but the most PFS-distal mutations (Extended Data Fig. 6), supporting the specificity of target-dependent activation. Importantly, a *GFP*-targeting GeCas12a2 RNP eliminated both *GFP*-expressing cell lines, even if depletion was stronger in HeLa-GFP cells (Fig. 4c). Therefore, Cas12a2 can be applied to selectively eliminate cells expressing transcripts from an integrated virus.

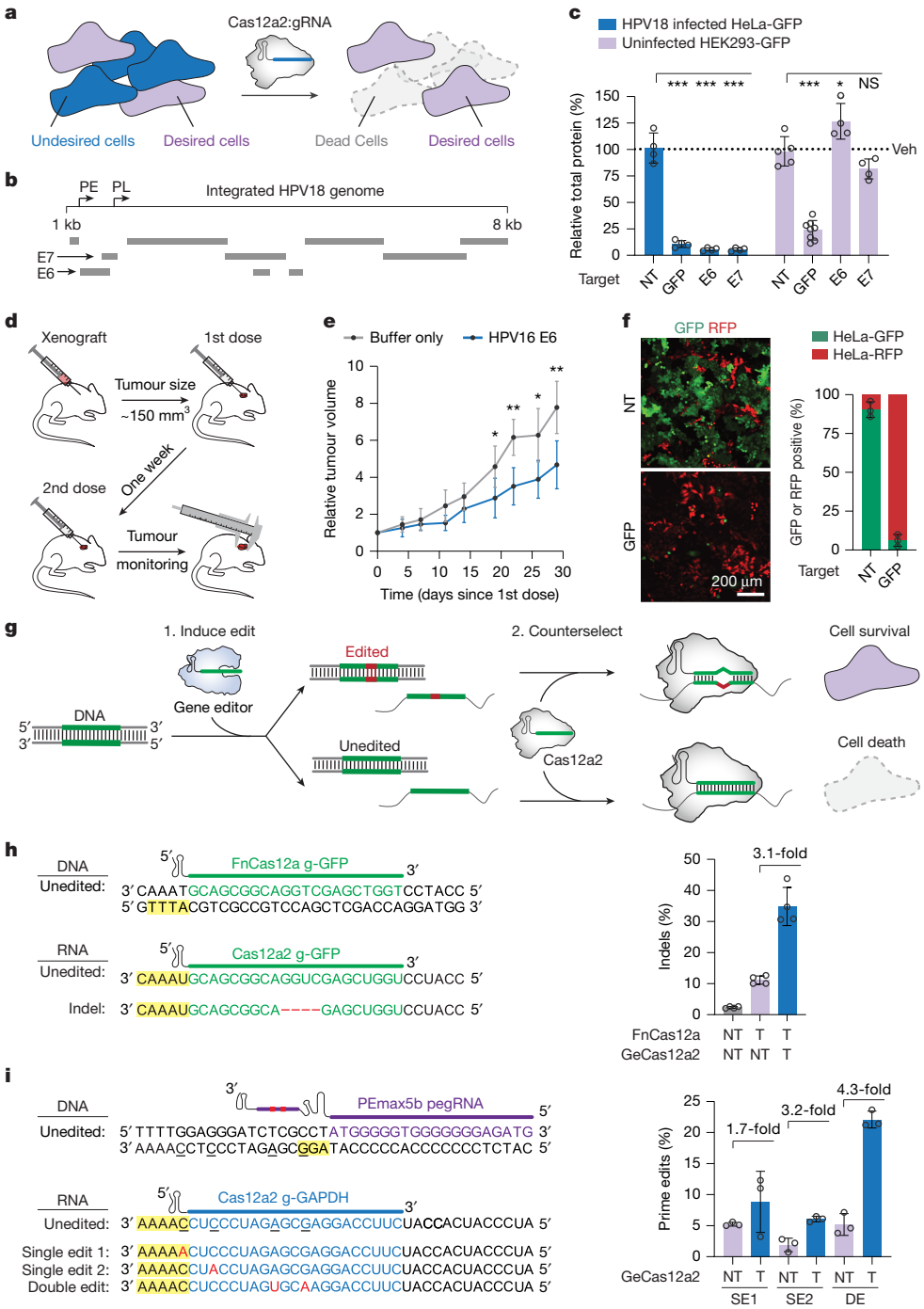


Fig. 4 | Cas12a2 selectively removes HPV-harbouring cells and enriches for gene-edited cells. a, Overview of using Cas12a2 to eliminate undesired cells while sparing desired cells in eukaryotes on the basis of transcriptional profiles. **b**, Targeting within the *E6* transcript of HPV18. PE and PL represent early and late viral promoters, respectively. **c**, Cell quantification by SRB following electroporation with GeCas12a2 against the indicated targets in HPV18-positive HeLa-GFP cells or HEK293-GFP cells, normalized to vehicle. **d**, Schematic of the in vivo mouse experiments. **e**, Reduction of an implanted HPV16-infected tumour in mice following the procedure in **d**. Tumour volumes are normalized for each animal to its individual tumour size at the first dose. Circles and error bars represent the mean and s.d. from five mice, respectively. **f**, Representative fluorescence microscopy and cell quantification by flow cytometry of a co-culture of HeLa-GFP and HeLa-RFP cells following electroporation with GeCas12a2 against the indicated targets. Images are representative of three biological replicates. **g**, Assessing the capacity of Cas12a2 to enrich for gene-edited cells through counterselection. **h**, Enriching indels in the heterologous *GFP* gene created by FnCas12a. The same gRNA was used for both FnCas12a and GeCas12a2. The red dashes represent the potential indels produced from FnCas12a2 editing. Quantification of indel frequency by Sanger sequencing when performing FnCas12a edits followed by introduction of GeCas12a2 in HeLa-GFP cells. NT, non-targeting gRNA. T, *GFP*-targeting gRNA. **i**, Enriching prime edits in the endogenous *GAPDH* gene created by Cas9-based prime editor. Underlining indicates prime editing sites; red text highlights the intended nucleotide substitution upon prime editing. Quantification of edit frequency by nanopore sequencing when performing PEmax5 or 5b edits followed by introduction of GeCas12a2 in HEK293-GFP cells. NT, non-targeting gRNA. T, *GAPDH*-targeting gRNA. SE, single-base edit. DE, double-base edit. Circles in **c**,**f**,**h** and **i** represent biological replicates ($n = 3$, 4 or 8), bars and error bars represent the mean and s.d. Two-tailed unpaired *t*-test with Welch's correction was performed; NS, $P > 0.05$; $^{*}P < 0.05$; $^{**}P < 0.01$; $^{***}P < 0.001$.

As a further extension, we assessed the capacity of GeCas12a2 to eliminate HPV-harbouring cells in vivo. Patient-derived cancer cells isolated from head and neck squamous cell carcinoma (HNSCC) were used to establish a patient-derived-xenograft flank mouse model to evaluate the effect of GeCas12a2 on tumour growth. The HNSCC isolate carried high-risk HPV variant 16 (HPV16); therefore, an *E6*-targeting gRNA against this variant was validated in SiHa cells for HPV16-specific cell depletion (Extended Data Fig. 7a,b). Intratumoural administration of LNP-packaged GeCas12a2 mRNA together with the HPV16 *E6*-targeting gRNA resulted in a significant reduction in tumour growth compared with the buffer-only control (Fig. 4d,e). Histology confirmed that GeCas12a2 was expressed, and the cells had apoptotic markers after 72 h (Extended Data Fig. 7c,d), paralleling the timeframe of apoptotic marker appearance in cell culture following administration of GeCas12a2 (Fig. 2d–g). Cas12a2 can therefore be implemented to eliminate target cells in vivo.

Cas12a2 enriches gene-edited cells

For the second scenario, we envisioned using Cas12a2 to enrich genome-editing events. Although a broad range of editing modalities exist[44], efficiencies can be limited depending on the genomic loci, cell types and editing strategy. Targeting the unedited transcript such that the desired edit blocks Cas12a2 target recognition could enrich for editing events—regardless of the underlying editor. To first test whether Cas12a2 could deplete only a selected subpopulation of cells in a mixed culture, we used a co-culture of *RFP*-expressing HeLa cells and an excess of *GFP*-expressing HeLa cells. Electroporating a *GFP*-targeting GeCas12a2 RNP resulted in a 93% reduction of *GFP*-expressing cells, as confirmed by confocal microscopy and flow cytometry analysis (Fig. 4f and Supplementary Fig. 10). The desired HeLa-RFP cells continued to proliferate without noticeable fitness defects, reaching confluence. Thus, Cas12a2 can eliminate target cells without directly harming surrounding non-target cells.

Building on this result, we turned to the enrichment of gene-edited cells (Fig. 4g). We began with the simplest scenario: enrichment of insertions or deletions (indels) created using a DNA-cutting nuclease. We selected Cas12a, which can target the same sequence as Cas12a2 and is known to generate larger indels compared with Cas9 (ref. 28). Cells were initially treated with FnCas12a RNPs targeting the chromosomally integrated *GFP* gene, yielding approximately 11% indels across the population (Fig. 4h). The resulting mixed population was then treated with GeCas12a2 targeting the same site in the expressed transcript, and indel formation was again evaluated after seven days (Extended Data Fig. 8a). Targeting with GeCas12a2 enriched the indel frequency of the population by 3.1-fold, with a noticeable increase in larger indels (Fig. 4h and Extended Data Fig. 8b,c).

Beyond indel formation, we assessed the enrichment of precise edits created via prime editing[45]. The Cas9-based prime editor introduced a one- or two-base mutation into *GAPDH*, albeit at lower editing efficiencies (Fig. 4i). To enrich for this edit, GeCas12a2 was programmed to selectively target the unedited sequence within the *GAPDH* transcript (Fig. 4i). Following a procedure similar to that used to enrich Cas12a-mediated indels (Extended Data Fig. 8d), we enriched for prime-edited cells by up to 4.3-fold compared with the non-targeting GeCas12a2 control. Thus, Cas12a2 can enrich for DNA edits generated by different gene editors and editing modalities.

Cas12a2 eliminates oncogenic cells

In the third scenario, we sought to demonstrate Cas12a2's specificity for disease-causing mutations such as in cancer or in immunological and neurological disorders[46,47]. We hypothesized that Cas12a2 could be designed to selectively recognize a disease-linked RNA target with a single-nucleotide substitution while sparing its wild-type (WT) counterpart, driving selective elimination of cells expressing the mutated transcript.

As a case study, we selected the well-established oncogenic *KRAS*^{G12C} mutation, a single G-to-T substitution in *KRAS* gene that results in a glycine-to-cysteine substitution at codon 12 and causes constitutive 'pro-growth' signalling. To pursue the selective elimination of cells expressing *KRAS*^{G12C}, we used GeCas12a2 RNPs with 24-nt guides. Three gRNA candidates were empirically selected to target the G12C transcript but not the mismatch-containing WT transcript (Fig. 5a). Of these, only g-KRAS(2) yielded extensive DNA degradation with the *KRAS*^{G12C} transcript and no DNA degradation with the WT *KRAS* transcript in vitro (Fig. 5b) and thus was used for subsequent cellular tests.

Ideally, targeting the *KRAS*^{G12C} transcript with Cas12a2 eliminates cells with the mutation and spares cells lacking the mutation. To make a direct comparison, we engineered U2OS cells, which normally express about 11 copies of the WT *KRAS* transcript (Extended Data Fig. 9a,b), to stably overexpress *GFP* and either WT *KRAS* or *KRAS*^{G12C}. After confirming that the two engineered cell lines overexpress WT and G12C *KRAS* transcripts at equivalently high levels (Fig. 5c,d), we electroporated both cell lines with GeCas12a2 equipped with g-KRAS(2). Compared with the non-targeting control, this RNP depleted the *KRAS*^{G12C}-overexpressing cell line by 62% yet did not measurably deplete the WT *KRAS*-overexpressing cell line (Fig. 5e). There was also no detectable DNA damage by GeCas12a2 equipped with g-KRAS(2) in the WT *KRAS*-overexpressing cell line based on NHEJ-mediated integration of the dsDNA barcode (Fig. 5f). Thus, GeCas12a2 can selectively eliminate cells harbouring the *KRAS*^{G12C} point mutation, even under conditions in which the WT *KRAS* is highly overexpressed.

We next targeted the *KRAS*^{G12C} mutation in NCI-H23 cells naturally harbouring this mutation in one allele and widely used in *KRAS* and cancer research[48,49]. The delivered GeCas12a2-g-KRAS(2) RNP resulted in 50% depletion of this cell line and—on the basis of an increase in 53BP1 foci—yielded DNA damage (Fig. 5g,h). The surviving cells did not have a significant decrease in *KRAS* transcript levels (Extended Data Fig. 9c,d), arguing against escape through a subpopulation of underexpressing cells. As cancers harbouring the *KRAS*^{G12C} mutation are clinically treated using the US Food and Drug Administration (FDA)-approved small-molecule drug sotorasib[50], we asked whether Cas12a2 could offer a complementary treatment strategy. Treatment with sotorasib alone depleted NCI-H23 cells by 65%, whereas combining sotorasib with GeCas12a2 synergized cell depletion to over 85% compared with a negative control (Fig. 5i). Furthermore, the same cell line cultured to become resistant to sotorasib (Supplementary Fig. 11), an emerging clinical issue linked to modulation of Wnt/β-catenin signalling[48,49], were depleted by 51% with GeCas12a2 (Fig. 5j). We obtained similar results when stably expressing SuCas12a2 fused to two NLSs in NCI-H23 cells and transfected with gRNAs, which revealed that serial gRNA doses could further boost cell depletion (Supplementary Fig. 12). In total, these results show that Cas12a2 can selectively deplete target cells harbouring a somatic point mutation and deplete cancer cells that have acquired resistance to an FDA-approved anticancer drug.

Discussion

Here we found that the indiscriminate dsDNA shredding activity of Cas12a2 nucleases can drive the elimination of yeast and human cells when unleashed by the specific targeting of a present transcript. Cells were eliminated by targeting transcripts with different cellular abundances (Fig. 1h), whereas cells lacking a target transcript were spared. Interrogating the basis of cell elimination in human cells revealed that Cas12a2 generates extensive chromosomal dsDNA breaks followed by cell cycle arrest and principally apoptotic cell death. By contrast, cells lacking the target RNA sequence did not have any measurable increase in dsDNA breaks and proliferated similarly to untreated cells, whether in isolation or in co-culture with targeted cells. Building on this discovery, we applied Cas12a2 to selectively eliminate cells on the basis of unique features of their transcriptional profile. Although transcript-mediated

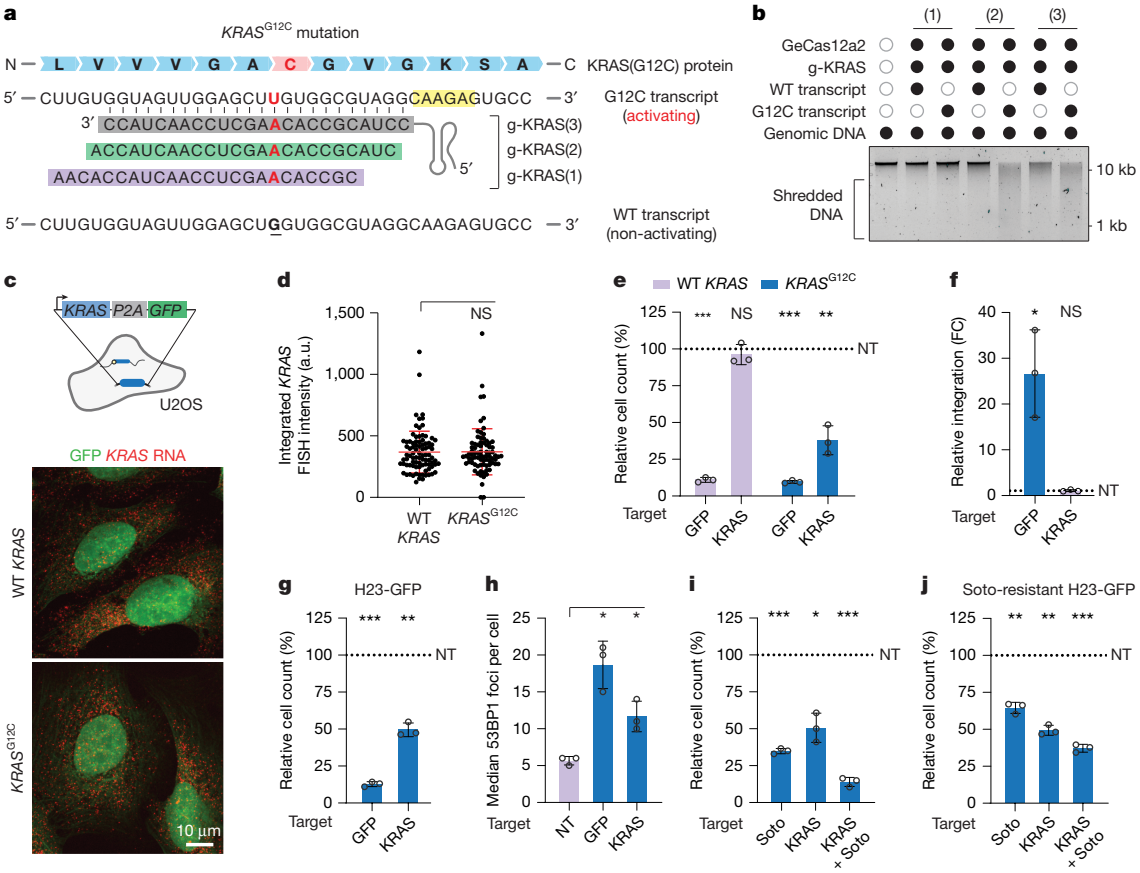


Fig. 5 | Cas12a2 selectively eliminates cancer cells by targeting a somatic point mutation. a, Targeting the G12C point mutation in the *KRAS* transcript. **b**, Cleavage of purified HeLa-GFP genomic DNA by GeCas12a2 and three gRNA candidates against the WT and G12C transcripts in vitro. g-KRAS, $KRAS^{G12C}$-targeting gRNA. Representative of three independent experiments. **c**, Expression construct and overlaid images of exogenously expressed WT *KRAS*-P2A-GFP or $KRAS^{G12C}$-P2A-GFP transcripts (red) and GFP proteins (green) in U2OS cells. Representative of three biological replicates. **d**, Quantification of exogenous WT *KRAS* or $KRAS^{G12C}$ transcript levels in U2OS cells by integrated RNA fluorescence in situ hybridization (FISH) signal intensity. Circles represent individual cells ($n = 87$ for WT *KRAS*, 79 for $KRAS^{G12C}$). **e**, Cell quantification by GFP fluorescence imaging (GFP object count) following electroporation with GeCas12a2 against the indicated targets in U2OS cells stably expressing WT *KRAS* or $KRAS^{G12C}$ transcripts quantified in **d**, normalized to non-target. **f**, Quantification of dsODN integration by qPCR following electroporation with GeCas12a2 against the indicated targets in U2OS cells stably expressing WT *KRAS*, normalized to non-target. **g**, Cell quantification by GFP fluorescence imaging (GFP object count) following electroporation with GeCas12a2 against the indicated targets in NCI-H23-GFP cells naturally harbouring heterozygous $KRAS^{G12C}$ mutations, normalized to non-target. **h**, Quantification of median 53BP1 foci per cell 24 h following electroporation with GeCas12a2 RNPs against the indicated targets in NCI-H23-GFP cells, normalized to vehicle (110–185 total cells analysed per condition). **i**, Cell quantification by phase contrast imaging following electroporation of GeCas12a2 RNPs against the indicated targets, treatment with 5 μM FDA-approved $KRAS^{G12C}$ covalent inhibitor sotorasib, or in combination with NCI-H23-GFP cells. **j**, Cell quantification by phase contrast imaging following treatment with GeCas12a2 RNPs and 5 μM sotorasib individually or together with sotorasib-resistant NCI-H23-GFP cells. Circles in **e**,**f**,**g**–**j** represent biological replicates ($n = 3$), bars and error bars represent the mean and s.d. Two-tailed unpaired *t*-test with Welch's correction was performed; NS, $P > 0.05$; $^*P < 0.05$; $^{**}P < 0.01$; $^{***}P < 0.001$.

cell depletion was primarily demonstrated in yeast and human cell lines, we expect the technique to extend to other eukaryotes, including additional animals and fungi as well as protists and plants.

Cas12a2-mediated cell killing differs from existing CRISPR and non-CRISPR approaches aiming to eliminate cells on the basis of their genetic and transcriptional identity. Existing CRISPR-based approaches are heavily restricted; for example, Cas9 requires highly repetitive DNA elements and is insensitive to gene expression[13]; Cas13 has limited efficacy when dependent on gene expression[9]; and the CRISPR-associated protease system involves multisubunit complexes that may limit its in vivo applicability[51]. Beyond CRISPR, numerous approaches could link the presence of a cellular RNA of interest in eukaryotic cells to induction of cell death, such as RNA-triggered riboregulators, microRNA-regulated expression constructs, *trans*-splicing ribozymes, or constructs that remove a premature start codon through RNA editing[52–57]. Among these approaches, to the best of our knowledge, only one has been used to enact cell death in eukaryotes in response to a target transcript[52], but with activity in the absence of a target, the inability to readily distinguish single-nucleotide polymorphisms, and a propensity for off-target RNA editing. By contrast, Cas12a2 can enact potent cell killing only in the presence of a recognized transcript, can achieve single-nucleotide resolution specificity, and can be triggered by poorly expressed transcripts. Thus, Cas12a2-mediated cell elimination represents a unique and important entry into the CRISPR–Cas toolbox for triggering cell death in response to selected transcripts.

We envision Cas12a2 being used against several types of RNA targets, including exogenous RNAs (for example, RNA viruses), expressed non-native genes, unique RNA fusions (for example, alternate splice junctions and circular RNAs), RNAs with acquired mutations (for example, single-nucleotide polymorphisms), and chemically modified RNAs (for example, A-to-I edits). The capability to target these diverse RNA types through facile gRNA design (Extended Data Fig. 3) can drive numerous applications in basic research, medicine, biotechnology, biomanufacturing and agriculture. We specifically demonstrated three

distinct applications by eradicating cells: (1) harbouring high-risk variants of HPV; (2) failing to undergo indel formation or prime editing; (3) harbouring a somatic oncogenic mutation. Gene editing enrichment could be extended to other editing strategies and in high-throughput CRISPR-based screens, although approaches producing undesired edits will require more development to specifically enrich for the desired edits (for example, HDR enrichment may be limited to genomic loci where indel formation is infrequent). Separately, Cas12a2 could be explored in gene drives to link cell killing to gamete formation or sex selection. Overall, we expect Cas12a2 to enable many more applications awaiting exploration.

Cas12a2-mediated cell elimination calls for a distinct approach to off-targeting analyses. For DNA-targeting nucleases such as Cas9, off-target analyses involve probing genomic sites resembling the target or undergoing DNA cleavage or repair[40,43]. For RNA-targeting nucleases such as Cas13d, off-target analyses involve predicting transcripts resembling the target that could undergo silencing[10,42]. For Cas12a2, the triggered nuclease is expected to generate dsDNA breaks indiscriminately throughout the genome regardless of the recognized RNA sequence, diminishing the utility of mapping off-target cleavage or transcript downregulation. Instead, we propose a combination of computational prediction of potential off-target activators, in vitro testing and detection of DNA damage and markers of cell death in relevant cell lines. Future work could extend this approach with high-throughput screening and machine learning to inform off-target prediction as well as systematically exploring means to further mitigate off-targeting[42,55].

Advances in CRISPR technologies over the past decade chart a clear path forward to advance Cas12a2-mediated cell elimination from a fledgling technique to a fully realized technology. This path includes changing or relaxing the adenine-rich PFS to accommodate more targets and facilitate targeting specificity sensitive to single point mutations, developing robust gRNA design rules based on high-throughput screens and machine learning, engineering more compact, active or higher-fidelity nucleases, and coupling Cas12a2 with viral and non-viral delivery vehicles for in vivo studies and therapies. A better understanding of contributing factors beyond Cas12a2 and guide design will also help to advance the technology, such as how the abundance and localization of target transcripts affect Cas12a2 activation and cell elimination, or how different cell types respond to the damage caused by triggered Cas12a2. Investigating cells that survive exposure to activated Cas12a2 would be particularly insightful depending on the extent of DNA repair and any resulting sequence, chromosomal and epigenetic changes. Finally, delineating the process of cell death in different cell types and the localized as well as systemic effect on the organism could contribute to therapeutic applications. For instance, Cas12a2-induced cell death in association with damage-associated molecular patterns may drive localized immune activation and help to clear cancer cells that evade direct targeting, similar to the use of oncolytic viruses[58]. Overall, with further investigation and development, Cas12a2 is poised to expand the CRISPR toolbox to incorporate programmable cell elimination in eukaryotic cells, opening a broad application space spanning the life sciences.

Online content

Any methods, additional references, Nature Portfolio reporting summaries, source data, extended data, supplementary information, acknowledgements, peer review information; details of author contributions and competing interests; and statements of data and code availability are available at https://doi.org/10.1038/s41586-026-10466-y.

1. Lam, K. N., Alexander, M. & Turnbaugh, P. J. Precision medicine goes microscopic: engineering the microbiome to improve drug outcomes. *Cell Host Microbe* **26**, 22–34 (2019).
2. Min, H.-Y. & Lee, H.-Y. Molecular targeted therapy for anticancer treatment. *Exp. Mol. Med.* **54**, 1670–1694 (2022).
3. Cappio Barazzone, E., Diard, M., Hug, I., Larsson, L. & Slack, E. Diagnosing and engineering gut microbiomes. *EMBO Mol. Med.* **16**, 2660–2677 (2024).
4. Vialetto, E. et al. Systematic interrogation of CRISPR antimicrobials in *Klebsiella pneumoniae* reveals nuclease-, guide- and strain-dependent features influencing antimicrobial activity. *Nucleic Acids Res.* **52**, 6079–6091 (2024).
5. Jiang, W., Bikard, D., Cox, D., Zhang, F. & Marraffini, L. A. RNA-guided editing of bacterial genomes using CRISPR-Cas systems. *Nat. Biotechnol.* **31**, 233–239 (2013).
6. Abudayyeh, O. O. et al. C2c2 is a single-component programmable RNA-guided RNA-targeting CRISPR effector. *Science* **353**, aaf5573 (2016).
7. Meeske, A. J., Nakandakari-Higa, S. & Marraffini, L. A. Cas13-induced cellular dormancy prevents the rise of CRISPR-resistant bacteriophage. *Nature* **570**, 241–245 (2019).
8. Li, Y. et al. The collateral activity of RfxCas13d can induce lethality in a RfxCas13d knock-in mouse model. *Genome Biol.* **24**, 20 (2023).
9. Shi, P. et al. Collateral activity of the CRISPR/RfxCas13d system in human cells. *Commun. Biol.* **6**, 334 (2023).
10. Abudayyeh, O. O. et al. RNA targeting with CRISPR-Cas13. *Nature* **550**, 280–284 (2017).
11. Ai, Y., Liang, D. & Wilusz, J. E. CRISPR/Cas13 effectors have differing extents of off-target effects that limit their utility in eukaryotic cells. *Nucleic Acids Res.* **50**, e65 (2022).
12. Schindele, A. et al. Using CRISPR-Kill for organ specific cell elimination by cleavage of tandem repeats. *Nat. Commun.* **13**, 1502 (2022).
13. Tan, I.-L. et al. Targeting the non-coding genome and temozolomide signature enables CRISPR-mediated glioma oncolysis. *Cell Rep.* **42**, 113339 (2023).
14. Tavella, S. et al. Weaponizing CRISPR/Cas9 for selective elimination of cells with an aberrant genome. *DNA Repair* **149**, 103840 (2025).
15. Dmytrenko, O. et al. Cas12a2 elicits abortive infection through RNA-triggered destruction of dsDNA. *Nature* **613**, 588–594 (2023).
16. Bravo, J. P. K. et al. RNA targeting unleashes indiscriminate nuclease activity of CRISPR-Cas12a2. *Nature* **613**, 582–587 (2023).
17. Hänggi, K. & Ruffell, B. Cell death, therapeutics, and the immune response in cancer. *Trends Cancer* **9**, 381–396 (2023).
18. Shkarina, K. & Broz, P. Selective induction of programmed cell death using synthetic biology tools. *Semin. Cell Dev. Biol.* **156**, 74–92 (2024).
19. Strathdee, S. A., Hatfull, G. F., Mutalik, V. K. & Schooley, R. T. Phage therapy: from biological mechanisms to future directions. *Cell* **186**, 17–31 (2023).
20. Shalhout, S. Z., Miller, D. M., Emerick, K. S. & Kaufman, H. L. Therapy with oncolytic viruses: progress and challenges. *Nat. Rev. Clin. Oncol.* **20**, 160–177 (2023).
21. Koonin, E. V. & Makarova, K. S. Evolutionary plasticity and functional versatility of CRISPR systems. *PLoS Biol.* **20**, e3001481 (2022).
22. Bikard, D. et al. Exploiting CRISPR-Cas nucleases to produce sequence-specific antimicrobials. *Nat. Biotechnol.* **32**, 1146–1150 (2014).
23. Citorik, R. J., Mimee, M. & Lu, T. K. Sequence-specific antimicrobials using efficiently delivered RNA-guided nucleases. *Nat. Biotechnol.* **32**, 1141–1145 (2014).
24. Gomaa, A. A. et al. Programmable removal of bacterial strains by use of genome-targeting CRISPR-Cas systems. *mBio* **5**, e00928 (2014).
25. Kiga, K. et al. Development of CRISPR-Cas13a-based antimicrobials capable of sequence-specific killing of target bacteria. *Nat. Commun.* **11**, 2934 (2020).
26. Cong, L. et al. Multiplex genome engineering using CRISPR/Cas systems. *Science* **339**, 819–823 (2013).
27. Mali, P. et al. RNA-guided human genome engineering via Cas9. *Science* **339**, 823–826 (2013).
28. Zetsche, B. et al. Cpf1 is a single RNA-guided endonuclease of a class 2 CRISPR-Cas system. *Cell* **163**, 759–771 (2015).
29. Smirnov, M. N., Smirnov, V. N., Budowsky, E. I., Inge-Vechtomov, S. G. & Serebrjakov, N. G. Red pigment of adenine-deficient yeast Saccharomyces cerevisiae. *Biochem. Biophys. Res. Commun.* **27**, 299–304 (1967).
30. Mao, Z., Bozzella, M., Seluanov, A. & Gorbunova, V. DNA repair by nonhomologous end joining and homologous recombination during cell cycle in human cells. *Cell Cycle* **7**, 2902–2906 (2008).
31. Scully, R., Panday, A., Elango, R. & Willis, N. A. DNA double-strand break repair-pathway choice in somatic mammalian cells. *Nat. Rev. Mol. Cell Biol.* **20**, 698–714 (2019).
32. Bot, J. F. et al. Temporal dynamics of collateral RNA cleavage by LbuCas13a in human cells. *Commun. Biol* https://doi.org/10.1038/s42003-026-09511-3 (2026).
33. Dimitrova, N., Chen, Y.-C. M., Spector, D. L. & de Lange, T. 53BP1 promotes non-homologous end joining of telomeres by increasing chromatin mobility. *Nature* **456**, 524–528 (2008).
34. Roos, W. P. & Kaina, B. DNA damage-induced cell death: from specific DNA lesions to the DNA damage response and apoptosis. *Cancer Lett.* **332**, 237–248 (2013).
35. Muslimović, A., Nyström, S., Gao, Y. & Hammarsten, O. Numerical analysis of etoposide induced DNA breaks. *PLoS ONE* **4**, e5859 (2009).
36. Roos, W. P., Thomas, A. D. & Kaina, B. DNA damage and the balance between survival and death in cancer biology. *Nat. Rev. Cancer* **16**, 20–33 (2016).
37. Huang, X., Tran, T., Zhang, L., Hatcher, R. & Zhang, P. DNA damage-induced mitotic catastrophe is mediated by the Chk1-dependent mitotic exit DNA damage checkpoint. *Proc. Natl Acad. Sci. USA* **102**, 1065–1070 (2005).
38. Plesca, D., Mazumder, S. & Almasan, A. DNA damage response and apoptosis. *Methods Enzymol.* **446**, 107–122 (2008).
39. Swanson, K. V., Deng, M. & Ting, J. P.-Y. The NLRP3 inflammasome: molecular activation and regulation to therapeutics. *Nat. Rev. Immunol.* **19**, 477–489 (2019).
40. Wienert, B. et al. Unbiased detection of CRISPR off-targets in vivo using DISCOVER-Seq. *Science* **364**, 286–289 (2019).
41. Tsai, S. Q. & Joung, J. K. Defining and improving the genome-wide specificities of CRISPR-Cas9 nucleases. *Nat. Rev. Genet.* **17**, 300–312 (2016).
42. Wessels, H.-H. et al. Prediction of on-target and off-target activity of CRISPR-Cas13d guide RNAs using deep learning. *Nat. Biotechnol.* **42**, 628–637 (2024).
43. Tsai, S. Q. et al. GUIDE-seq enables genome-wide profiling of off-target cleavage by CRISPR-Cas nucleases. *Nat. Biotechnol.* **33**, 187–197 (2014).

44. Pacesa, M., Pelea, O. & Jinek, M. Past, present, and future of CRISPR genome editing technologies. *Cell* **187**, 1076–1100 (2024).
45. Anzalone, A. V. et al. Search-and-replace genome editing without double-strand breaks or donor DNA. *Nature* **576**, 149–157 (2019).
46. Vogelstein, B. et al. Cancer genome landscapes. *Science* **339**, 1546–1558 (2013).
47. Sønderby, I. E. et al. Effects of copy number variations on brain structure and risk for psychiatric illness: large-scale studies from the ENIGMA working groups on CNVs. *Hum. Brain Mapp.* **43**, 300–328 (2022).
48. Mohanty, A. et al. Acquired resistance to KRAS G12C small-molecule inhibitors via genetic/nongenetic mechanisms in lung cancer. *Sci. Adv.* **9**, eade3816 (2023).
49. Rosell, R. et al. KRAS G12C-mutant driven non-small cell lung cancer (NSCLC). *Crit. Rev. Oncol. Hematol.* **195**, 104228 (2024).
50. Nakajima, E. C. et al. FDA approval summary: sotorasib for KRAS G12C-mutated metastatic NSCLC. *Clin. Cancer Res.* **28**, 1482–1486 (2022).
51. He, M. et al. A synthetic system for RNA-responsive pyroptosis based on type III-E CRISPR nuclease-protease. *Nat. Commun.* https://doi.org/10.1038/s41467-026-69179-5 (2026).
52. Jiang, K. et al. Programmable eukaryotic protein synthesis with RNA sensors by harnessing ADAR. *Nat. Biotechnol.* **41**, 698–707 (2023).
53. Kaseniit, K. E. et al. Modular, programmable RNA sensing using ADAR editing in living cells. *Nat. Biotechnol.* **41**, 482–487 (2023).
54. Yarra, S. S., Ashok, G. & Mohan, U. 'Toehold switches; a foothold for synthetic biology'. *Biotechnol. Bioeng.* **120**, 932–952 (2023).
55. Shivram, H., Cress, B. F., Knott, G. J. & Doudna, J. A. Controlling and enhancing CRISPR systems. *Nat. Chem. Biol.* **17**, 10–19 (2021).
56. Han, S. R. et al. Targeted suicide gene therapy for liver cancer based on ribozyme-mediated RNA replacement through post-transcriptional regulation. *Mol Ther. Nucleic Acids* **23**, 154–168 (2021).
57. Hong, S.-H. et al. In vivo reprogramming of hTERT by trans-splicing ribozyme to target tumor cells. *Mol. Ther.* **16**, 74–80 (2008).
58. Lichty, B. D., Breitbach, C. J., Stojdl, D. F. & Bell, J. C. Going viral with cancer immunotherapy. *Nat. Rev. Cancer* **14**, 559–567 (2014).

Publisher's note Springer Nature remains neutral with regard to jurisdictional claims in published maps and institutional affiliations.

Open Access This article is licensed under a Creative Commons Attribution-NonCommercial-NoDerivatives 4.0 International License, which permits any non-commercial use, sharing, distribution and reproduction in any medium or format, as long as you give appropriate credit to the original author(s) and the source, provide a link to the Creative Commons licence, and indicate if you modified the licensed material. You do not have permission under this licence to share adapted material derived from this article or parts of it. The images or other third party material in this article are included in the article's Creative Commons licence, unless indicated otherwise in a credit line to the material. If material is not included in the article's Creative Commons licence and your intended use is not permitted by statutory regulation or exceeds the permitted use, you will need to obtain permission directly from the copyright holder. To view a copy of this licence, visit http://creativecommons.org/licenses/by-nc-nd/4.0/.

© The Author(s) 2026

Methods

Phylogenetic analysis

The amino acid sequence of GeCas12a2 was aligned with other Cas12a2 nuclease sequences[15,59] using Clustal Omega[60]. The alignment was trimmed with ClipKIT[61] and used to reconstruct a phylogeny with IQ-TREE v2.0.3 (-m MFP -T 8 -B 1000)[62], using a maximum-likelihood approach. The phylogeny included Cas12a orthologues and used Cas12c as an outgroup. Branch confidence was reported as ultrafast bootstrap values (ranging from 0 to 100).

PFS library preparation

A PFS-containing plasmid library (CBS-6873) was constructed to include a target sequence (Supplementary Tables 8 and 9) followed by five randomized nucleotides (NNNNN). The target sequence was placed under a PJ23119 promoter and cloned into a low-copy sc101 origin plasmid (about five copies per cell). The library was generated by amplifying a target-encoding plasmid with primers ODpr23 and ODpr24 (Supplementary Tables 9 and 10). The forward primer contained a 5-nt randomized overhang. The PCR product was treated with DpnI to remove template DNA, ligated, and electroporated into *Escherichia coli* (*E. coli*) TOP10, yielding over two million transformants (approximately 2,000-fold library coverage).

PFS library depletion

The PFS preference of the GeCas12a2 nuclease (CBS-6874) was assessed by targeting the CBS-6873 PFS plasmid library with a CAO1-targeting CRISPR RNA (crRNA) plasmid (CBS-6875) or a non-targeting crRNA plasmid (CBS-6876). The GeCas12a2 nucleotide sequence was codon-optimized for expression in *E. coli*. The nuclease-encoding sequence was under a T7 promoter, whereas crRNA was expressed from PJ23119. *Escherichia coli* BL21(AI) cells containing nuclease and crRNA plasmids were electroporated with the PFS plasmid library. Each electroporation used approximately 500 ng of library plasmid DNA in 50 µl competent cells, followed by recovery in lysogeny broth medium containing 0.1 mM isopropyl β-D-1-thiogalactopyranoside (IPTG) and 0.2% L-arabinose. Overnight cultures (of approximately two million transformants) ensured greater-than-2,000-fold library coverage. Plasmids were purified with ZymoPURE II Plasmid Midiprep Kit (D4201).

PFS library sequencing and analysis

Purified plasmids from targeting and non-targeting conditions were PCR-amplified using primers ODpr55 and ODpr56 (Supplementary Table 10) with KAPA HIFI HotStart polymerase (KK2601) for 20 cycles at 64.5 °C, following the manufacturer's protocol. Indexed PCR products were sequenced on Illumina NovaSeq 6000 (paired-end, 150 bp reads), at least two million reads each. Raw FASTQ files were processed with Trimmomatic v.0.39 (parameters: ILLUMINACLIP:TruSeq3-PE.fa:2:30:10, LEADING:3, TRAILING:3, SLIDINGWINDOW:4:15). Paired-end reads were merged with BBMerge (qtrim = t trimq = 10 minlength = 20). Sequences containing motifs matching TTCCTTCAGGTGTTGCTCCA(.....)GGTGAGTTCT were extracted, excluding sequences with N bases or Phred scores of below 20. Depletion scores were calculated using the following formula: depletion = sum(non-target)/sum(target) × count(target)/count(non-target). $\log_2$ fold-change values for depletion scores were computed for nucleotides at PFS positions (−1 to −5). Scatterplots visualizing PFS preferences were generated using Matplotlib in Python.

Coexpression of gRNA and FLAG-tagged GeCas12a2 or FLAG-tagged FnCas12a

Electrocompetent *E. coli* BW25113 cells were transformed with a GeCas12a2-FLAG expression plasmid and a plasmid containing the gRNA's sequence (Supplementary Table 9). Newly transformed cells were grown on lysogeny broth agar plates containing 25 µg ml^{-1} kanamycin (Kan) and 100 µg ml^{-1} ampicillin (Amp) for 12–16 h at 37 °C. A single colony was selected and used to start an overnight culture, from which a 120 ml culture of lysogeny broth–Amp–Kan medium was inoculated to a starting OD_{600} of 0.05, and then incubated at 37 °C at 200 r.p.m. When OD_{600} = 0.2 was reached, the cultivation temperature was lowered from 37 °C to 21 °C. Once the growth reached an OD_{600} of 0.5, expression was induced by adding L-arabinose (to a final concentration of 0.2%). Cells were collected by centrifugation after 16–18 h at 21 °C.

Purification of FLAG-tagged GeCas12a2 or FnCas12a–gRNA RNP complex

Escherichia coli cell pellets (90 optical density volumes) were resuspended in 3 ml Tris-buffered saline (TBS) (150 mM NaCl, 50 mM Tris/HCl pH7.4) containing a mix of protease inhibitors (Complete, ethylenediaminetetraacetic acid-free; Sigma Aldrich), and then lysed by sonication on ice (Branson Sonifier 250 with four ultrasonic cycles, 50% duty cycle, 2.5 output for 30 s). The lysate was cleared by centrifugation (5,525 × *g* for 10 min at 4 °C) and filtered through a 0.22 µm polyethersulfone membrane (Merck Chemicals). The cleared lysate was divided into two 1.5 ml aliquots and added to 120 µl of magnetic anti-FLAG beads (Pierce Anti-DYKDDDDK magnetic agarose; Thermo Fisher Scientific) that were pre-washed twice with TBS buffer. The lysate was incubated with the magnetic anti-FLAG beads overnight on a rotating wheel at 4 °C, allowing the FLAG-tagged RNP complexes to bind to the magnetic anti-FLAG beads. The magnetic beads were then washed three times with ice-cold TBS buffer and once with double-distilled water (with the magnetic beads fixed to a magnetic rack in between each wash). The supernatant was completely removed, and the FLAG-tagged RNPs were eluted using 1.5 mg ml^{-1} of a triple FLAG peptide (Pierce 3×DYKDDDDK Peptide; Thermo Fisher Scientific) resuspended in 50 µl phosphate-buffered saline (PBS) (Dulbecco's PBS without Ca^{2+} and Mg^{2+}; PAN Biotech) on a slowly shaking platform for 30 min at room temperature. The purified FLAG-tagged RNPs were collected by fixing the magnetic beads in a magnetic rack and pipetting out the supernatant. The purified RNPs were quantified by measuring the absorbance at 280 nm (DeNovix reader), before being stored at 4 °C.

Expression of apo and catalytically dead GeCas12a2 and SuCas12a2

Apo GeCas12a2 and apo SuCas12a2 were expressed similarly to the expression method of SuCas12a2 described in a past work[16]. In brief, the *gecas12a2* gene sequence was cloned into a 2S-T pET plasmid in frame with an N-terminal HIS-SUMO tag. SuCas12a2 was cloned into a pACYC plasmid with a N-term-hexa HIS tag. Both plasmids were separately transformed into chemically competent *E. coli* HMS-174(DE3) cells. Protein expression for GeCas12a2 and SuCas12a2 was performed using similar methods. A single colony was used to inoculate 60 ml of lysogeny broth medium for an overnight (16–18 h) growth at 37 °C with shaking at 200 r.p.m. The starter growth (20 ml) was then used to inoculate 1 l lysogeny broth medium containing 100 µg ml^{-1} ampicillin. The 1 l cultures were grown to an OD_{600} of 0.5–0.6 at 37 °C, and then cold shocked on ice for 20 min before being induced with 0.1 mM IPTG; this was followed by growing the cells for 16–18 h at 18 °C. Cell pellets were collected by centrifugation and stored at −80 °C.

Purification of apo and catalytically dead GeCas12a2 and SuCas12a2

Apo GeCas12a2/Ge(d)Cas12a2 and apo SuCas12a2 were purified similarly to the purification method of SuCas12a2 outlined in a previous work[16]. In brief, collected cell pellets were thawed on ice for 20 min before being resuspended in 50 ml of lysis buffer (25 mM Tris pH 7.2, 500 mM NaCl, 2 mM MgCl2, 10 mM imidazole, 10% glycerol) containing protease inhibitors (2 µg ml^{-1} aprotinin, 10 µM leupeptin, 1.0 µg ml^{-1} pepstatin) and 1 mg ml^{-1} lysozyme; they were then incubated for 20 min on ice with gentle rocking. Cells were further lysed by sonication (at

3/50 for 25 min) and clarified by centrifugation at 36,400 *g* for 35 min. Clarified lysate was added to 5 ml of Ni-NTA resin and batch bound at 4 °C for 30 min, followed by running the lysate over the resin for a second time. The resin was washed with 500 ml of Ni-NTA wash buffer (25 mM Tris pH 7.2, 2 M NaCl, 2 mM $MgCl_2$, 10 mM imidazole, 10% glycerol) and eluted with nickel elution buffer (25 mM Tris pH 7.2, 500 mM NaCl, 2 mM $MgCl_2$, 250 mM imidazole, 10% glycerol). Using a HiPrep 26/10 desalting column (Cytiva), elutions from the nickel column were desalted into low-salt buffer (25 mM Tris pH 7.2, 50 mM NaCl, 2 mM $MgCl_2$, 10% glycerol). GeCas12a2's low-salt buffer contained 200 mM, rather than 50 mM, NaCl to help with solubility. Furthermore, GeCas12a2 was treated for tag cleavage by adding 1:50 tobacco etch virus (TEV) protease and dithiothreitol (DTT) to GeCas12a2 for 2 h at room temperature. Both apo GeCas12a2 and apo SuCas12a2 were applied to a Hitrap SP HP cation-exchange column and eluted with a gradient of high-salt buffer (25 mM Tris pH 7.2, 1.0 M NaCl, 2 mM $MgCl_2$, 10% glycerol). Fractions containing apo GeCas12a2 or apo SuCas12a2 were concentrated to 1 ml using a 100 kDa MWKO concentrator. Concentrated protein was loaded over a HiLoad 26/600 Superdex 200 pg column using size-exclusion chromatography buffer (100 mM HEPES pH 7.2, 150 mM KCl, 2 mM $MgCl_2$, 10% glycerol). Peak fractions containing apo GeCas12a2 or apo SuCas12a2 were concentrated to a working concentration again using a 100 kDa MWKO concentrator before aliquoting and flash freezing with liquid nitrogen and stored at −80 °C.

FAM-labelled collateral cleavage assays

Collateral cleavage assays were performed as described previously[15]. In brief, 20 µl reactions containing 1× NEB 3.1 buffer (100 mM NaCl, 50 mM Tris-HCl, 10 mM $MgCl_2$, 100 µg ml^{-1} bis(trimethylsilyl)acetamide (BSA), pH 7.9) were made by combining 300 nM crRNA with 250 nM of GeCas12a2 or SuCas12a2, along with 100 nM of 5′-FAM labelled collateral substrate (ssDNA, dsDNA or ssRNA). Finally, 250 nM of target RNA was added to initiate the reaction and incubated at 37 °C for 1 h. Reactions were quenched with phenol, and nucleic acid was purified by phenol–chloroform extraction. The cleaved nucleic acid was analysed by 12% urea-polyacrylamide gel electrophoresis (urea-PAGE) and visualized for fluorescein fluorescence. Guide and target RNA were in vitro transcribed to determine dsDNA cleavage when targeting mRNA transcripts (GAPDH, EGFP, MALAT1, HPV18.6, HPV18.7).

Yeast cell culture and quantification

Chemically competent *S. cerevisiae* S288c cells were transformed using the high-efficiency lithium acetate/single-stranded carrier DNA/PEG method[63], using 1 µg of the nuclease/gRNA expression plasmid and 500 ng HDR-template (Supplementary Tables 11 and 12). Following regeneration, transformed cells were plated on selective yeast extract peptone dextrose agar plates containing 50 µg ml^{-1} geneticin (G418) and incubated for at least two days at 30 °C. The colonies were then counted and grouped according to their colour, with a successful knockout being determined by the red colour of the clone.

Mammalian cell culture

HeLa, HeLa-GFP, HeLa-RFP, HEK293T, HEK293-GFP, SiHa and U2OS cells were cultured in Dulbecco's modification of Eagle's medium (DMEM) supplemented with 10% serum, glucose, L-glutamine and sodium pyruvate. HeLa-GFP and HeLa-RFP cultures were supplemented with 10 µg ml^{-1} blasticidin (InvivoGen) and 2.5 µg ml^{-1} puromycin (InvivoGen), respectively, to maintain reporter selection. COR-L23 cells were cultured in RPMI 1640 medium supplemented with 10% serum and L-glutamine. SCC-4 cells were cultured in Ham's F12/DMEM (1:1) containing 20% serum, L-glutamine and 50 µg ml^{-1} hydrocortisone (Sigma-Aldrich). SK-MEL-30 were cultured in DMEM supplemented with 10% serum, glucose and 1× GlutaMAX (Fisher Scientific). PC3-GFP cells were cultured in F12K medium (Kaighn's modification) supplemented with 10% serum and L-glutamine. NCI-H23 cells were cultured in RPMI 1640 (ATCC Modification) supplemented with 10% serum, glucose, L-glutamine, sodium pyruvate and sodium bicarbonate. All media were further supplemented with broad spectrum antimicrobials and tested monthly for detection of mycoplasma. All cultures were incubated at 37 °C with 5% CO_2 (refer to Supplementary Table 8 for a complete list of cell lines and origins).

Electroporation of CRISPR RNPs to mammalian cells

Cells (1×10^5) were transfected with RNPs (GeCas12a2, SuCas12a2, LbuCas13a, FnCas12a) made by combining a 1:1 molar ratio of 50 pmol of nuclease and gRNA at room temperature for 30 min. For 5×10^5 and 1×10^6 cell reactions, 250 pmol of nuclease and gRNA were incubated together. The RNP complexes were transfected using the Neon and Neon NxT electroporation systems (Thermo Fisher Scientific). Device settings were: 1,300 V/30 ms/1 pulse for HeLa cell types; 1,200 V/40 ms/1 pulse for HEK293 cell types; 1,400 V/15 ms/2 pulses for U2OS cell types; 1,250 V/30 ms/1 pulse for PC3 cell types; and 1,400 V/30 ms/1 pulse for H23 cell types. COR-L23, SCC-4 and SK-MEL-30 cells were electroporated using the NEPA21 electroporator (Nepa Gene) with the following conditions: 150 V for 5 ms, 175 V for 5 ms and 150 V for 7.5 ms, respectively. After pulsing the cells, samples were plated according to assay type or further cultured for downstream treatment and analysis.

Imaging, cell counting and intensity quantification by Incucyte tracking

Following payload delivery, cells were seeded in 96-well or 24-well plates and live-imaged every 4 h for up to five days in phase contrast and, when relevant, GFP channels (300 ms acquisition) using the Incucyte SX5 system (Sartorius) and Incucyte Base Analysis Software (v2023A). Four to sixteen images were acquired per well, from which representative figures were prepared. Incucyte software-based cell quantifications include the phase contrast confluence, phase contrast object count per image, GFP object count per image and the total integrated GFP intensity per image (refer to Figs. 1e,g,i, 5e,g,i,j and Extended Data Fig. 4d,e).

Total cellular protein quantification by SRB

Cells in 96-well plates were fixed with 10% trichloroacetic acid for 30 min on ice and stained with 0.4% sulforhodamine B (Sigma Aldrich) in 1% acetic acid solution for 10 min at room temperature. After washing several times with 1% acetic acid, the 96-well plates were allowed to dry at room temperature. Sulforhodamine B dye was extracted by incubation in chilled 10 mM TRIS/HCl buffer (pH 10.5) for 15 min at 4 °C. Absorbance was measured at 550 nm in FlexStation 3 microplate reader (Molecular Devices) or BioTek Synergy Neo2 microplate reader (Agilent).

LbuCas13a in vitro guide verification

The activity of LbuCas13a (GenScript) was monitored by measuring the fluorescence intensity of cleaved RNase Alert Reporter Substrates (Thermo Fisher Scientific). LbuCas13a: guide complex was formed by incubating 1 µM LbuCas13a with 0.5 µM gRNA in Cas13a reaction buffer (GenScript) at 37 °C for 10 min. After the complex was formed, several reaction conditions were prepared in a 384 black bottom plate. The final reaction concentrations for each component were 100 nM LbuCas13a:50 nM guide complex, 50 nM Target RNA, 180 nM RNase Alert Substrate, 1× Cas13a reaction buffer and 15 nM of RNase A. The reaction was incubated for 45 min at 37 °C, followed by measuring the fluorescence intensity (excitation $\lambda_{ex.}$ = 485 nm and $\lambda_{em.}$ = 535 nm) using a BioTek Synergy H4 Hybrid plate reader. The background fluorescence was determined to be the reaction condition containing Cas13a buffer and RNase Alert Reporter, and was subtracted from the other reaction conditions.

RNA-seq analysis of transcript abundance

For the HeLa-GFP and HEK293-GFP cell lines, RNA sequencing and the fragments per kilobase of exon per million fragments mapped (FPKM) calculations were performed as described in a past work[64].

In brief, RNA isolation was performed using the NucleoSpin RNA Kit (Macherey-Nagel). The TruSeq RNA Library Prep Kit (v.2) from Illumina was used for library preparation, with an initial input amount of 500 ng of total RNA. The prepared libraries were sequenced with a 2 × 150 bp read length using the HiSeq 3000/4000 SBS Kit and an Illumina Hiseq 4000 sequencer. The adaptor trimmed, demultiplexed and quality filtered reads were aligned to the hg38 reference genome and transcriptome using Hisat2 (v.2.2.1). The Hisat2 output files (SAM) were converted to the BAM format and were sorted and indexed using SAMtools (v.1.3.1). The sorted BAM files were further processed using Cufflinks (v.2.1.1) to quantify the transcript abundances displayed in FPKM. For U2OS and NCI-H23 cell lines, RNA isolation was performed using the Quick-RNA Miniprep Kit (Zymo, R1054) according to the manufacturer's protocol. Read-pair libraries were created with the NEBNext Ultra II Directional RNA Library Prep with rRNA Depletion kit (New England Biolabs, E7760). Next-generation sequencing of samples was subsequently performed on the Illumina NovaSeq X Series 150 × 150 bp platform. Sequencing reads were aligned to the GRCh38 genome (hg38) using the STAR aligner (v2.7.11b) with a pre-built RSEM index[65]. The RSEM reference index was generated using gene annotations from Gencode v.33 and the GRCh38 genome. Transcript abundance was quantified by RSEM, reporting FPKM values (v1.2.28)[66]. The STAR-aligned genome BAM output was sorted and indexed using SAMtools (v1.16)[67].

LNP production and RNA delivery

LNPs were manufactured using Cytiva's Ignite+ system equipped with NxGen mixer to provide 0.2 mg of formulated payload. The formulations were downstream processed and concentrations were adjusted to 0.25 mg ml^{-1}. The mRNA and gRNA payload were co-packaged in a mass ratio of 60:40% (w/w). For the LNP application, HEK293T cells were seeded in 96-well plates. After 24 h, 40 ng of mRNA/gRNA-co-packaged LNPs were added to each 96-well containing ApoE3 (1 μg ml^{-1} final concentration, PeproTech) supplemented culture medium (DMEM containing 10% FCS and 4 mM Glutamine). After 6 h, the culture medium was replaced and the application of 40 ng mRNA/gRNA co-packaged LNPs was repeated. Confluence was quantified by Incucyte 72 h later.

Genomic DNA collateral cleavage assays

Collateral cleavage assays were performed as 10-μl reactions containing 0.1× NEB 3.1 buffer, 50 nM gRNA, 50 nM GeCas12a2, and nuclease-free water. After an initial 15-min incubation to form the RNP complex, 50 nM of target RNA were added to activate the complex. Approximately 50 ng of extracted genomic DNA (DNeasy Blood & Tissue Kit, Qiagen) was then added to each condition and samples incubated at 37 °C for 30 min. After 30 min, samples were treated with RNase A for 5 min and then Proteinase K for 10 min at 56 °C. Samples were visualized on a 1% TAE agarose gel run at 100 V for 40 min.

Immunofluorescence microscopy

GeCas12a2 or SuCas12a2 RNPs were delivered to 1×10^5 HeLa-GFP cells by electroporation which were then seeded onto glass coverslips and incubated for 18–24 h. Following incubation, samples were fixed with 4% paraformaldehyde in 1× PBS for 10 min then quenched with 100 mM glycine in 1× PBS for 10 min. Samples were rinsed with 1× PBS and subsequently permeabilized with 0.05% Triton-X in 1× PBS for 10 min. After an additional rinse with 1× PBS, samples were blocked with 2% BSA in 1× PBS for 1 h at room temperature. Following the block step and without rinsing, samples were treated with rabbit anti-53BP1 antibody (Novus Biologicals, NB100-306) diluted 1:1,000 in 1× PBS for 1 h at room temperature. Samples were then rinsed three times with 1× PBS before being treated with goat anti-rabbit Alexa Fluor 647 secondary antibody (Invitrogen, A32733) diluted 1:2,000 in 1× PBS for 1 h at room temperature. At the conclusion of the secondary incubation, samples were rinsed three times with 1× PBS waiting 5 min in between each rinse. Coverslips were mounted on glass slides using Prolong Diamond Antifade Mountant with DAPI (Thermo Fisher Scientific) overnight. Prepared samples were imaged using the Nikon Ti2 Eclipse confocal microscopy system with excitation of DAPI and 53BP1 fluorophore using 405 nm and 647 nm lasers, respectively. Raw images were exported from Nikon NIS-Elements software (v.5.41.02), split into individual channels using Fiji ImageJ software, and saved as .tif files. DAPI and 53BP1 channel images were then loaded into a custom CellProfiler pipeline to quantify the number of 53BP1 foci per cell.

Cell cycle analysis

Forty-eight hours after electroporation of GeCas12a2 or SuCas12a2 RNPs to 5×10^5 HeLa-GFP cells, cultures were suspended in 200 μl phenol red-free Leibovitz's L−15 medium followed by 200 μl of 4% PFA fixative and incubated on ice for 25 min. To remove fixative, cells were pelleted by centrifugation at 250 RCF for 5 min and washed with 500 μl L-15 twice. To stain genomic DNA, cells were pelleted again and resuspended in 500 μl of a 1× PBS solution with 10 μg ml^{-1} DAPI stain (BD Pharmingen, 564907) and 0.1% Triton-X for 15 min at room temperature followed by 10 min on ice. Cells were strained through a 35-μm mesh cap before analysis to ensure single cell suspension. Ten thousand cells per condition were analysed by flow cytometry using the BD FACSCelesta system with 405 nm laser excitation for DAPI. Data were analysed using FlowJo v.10.

Annexin-V and caspase-3/7 staining

Forty-eight hours after electroporation of GeCas12a2 or SuCas12a2 RNPs to 5×10^5 HeLa-GFP cells, cultures were washed with 1× PBS, treated with 0.05% trypsin, centrifuged, and resuspended in annexin-V binding buffer (10 mM HEPES, 140 mM NaCl, 2.5 mM $CaCl_2$, pH 7.4). For annexin V analysis, resuspended cells were mixed with Alexa Fluor 647 annexin-V antibody (BD Pharmingen, 567356) at a volumetric ratio of 1:40 and incubated at room temperature for 15–30 min. Immediately preceding data acquisition, samples were mixed with 10 μg ml^{-1} DAPI stain (BD Pharmingen, 564907) at a volumetric ratio of 1:80. For caspase-3/7 analysis, resuspended cells were mixed with 0.2 mM NucView 405 caspase-3/7 substrate (Biotium, 10407) at a volumetric ratio of 1:200 and incubated for 30 min at room temperature. Ten thousand cells per condition were analysed by flow cytometry using the BD FACSCelesta system with 405 nm laser excitation for DAPI or caspase-3/7 substrate and 640 nm laser excitation for annexin V. Data were analysed using FlowJo (v.10).

RNA-seq cell death pathway analysis

Forty-eight hours after electroporation of GeCas12a2 RNPs to 5×10^5 HeLa-GFP cells, total RNA was collected using Quick-RNA Miniprep Kit (Zymo, R1054) according to the manufacturer's protocol. Read-pair libraries were created with NEBNext Ultra II Directional RNA Library Prep with poly(A) mRNA isolation kit (New England Biolabs, E7760). Next-generation sequencing of samples was then performed on the Illumina NovaSeq X Series 150 × 150 bp platform with 25 million reads per condition. Sequencing reads were aligned to hg38 with Bowtie2 (v.2.2.9)[68]. Read counts for each GENCODE gene were quantified with RSEM (v.1.2.28)[66]. We used DESeq2 (v.1.44.0)[69] to normalize the read counts and perform differential expression analysis. We used the cut-off of padj <0.05 and fold change of >1.5 to identify genes significantly up- or downregulated between conditions indicated in the Article. Gene set enrichment analysis (v.4.3.3)[70] was run to determine the enriched gene sets. We used the R package fgsea (v.1.30.0)[71] to calculate the normalized enrichment statistics for each gene set in the Hallmark Collection from the Molecular Signatures Database[72].

qPCR of incorporated dsODN for off-target double-strand-break detection

Detection of dsDNA breaks by qPCR of integrated donor oligos (dsODN) is adapted from the GUIDE-Seq method as described

previously[73]. Amplicons were not sequenced in line with the full GUIDE-seq protocol, given expectations that the distribution of identified integration sites with the non-targeting guide would be difficult to distinguish from that of the vehicle-only control. One million cells were electroporated with 250 pmol of GeCas12a2 RNPs (or buffer) and 5 pmol of dsODN. The blunt-ended dsODN was prepared by annealing two single-stranded DNA oligos (dsODN_For/dsODN_Rev, Table S3). Forty-eight hours following electroporation, test conditions were collected for genome extraction using DNeasy Blood and Tissue Kit (Qiagen) according to the manufacturer's protocol. Four hundred ng of collected genomic DNA were digested into 300–700 bp fragments and end-repaired using NEBNext Ultra II FS DNA Module (NEB) according to manufacturer's protocol (10-min incubation at 37 °C). Reactions were purified using AMPure XP beads (Beckman Coulter) and ligated to adaptors (MNase_For/MNase_Rev, Table S3) with T4 Ligase (NEB). Reactions were purified using AMPure XP beads and PCR amplified with Illumina-based adaptors (PE_i5/PE_i7, Supplementary Table 3) using Q5 Master Mix (NEB). PCR-amplified samples were purified with AMPure XP beads before proceeding to qPCR on QuantStudio 3 (ThermoFisher) using Luna qPCR Master Mix (NEB) according to manufacturer's protocol. Total input DNA Ct was determined by qPCR of each sample diluted 1:250 with primers against the Illumina-based adaptors (P5/P7, Supplementary Table 3). Amplification of dsODN-specific DNA was determined by qPCR of each sample with primers against one Illumina-based adaptor and the known dsODN sequence (PdsODN_For/PdsODN_Rev, Supplementary Table 3). Resulting Ct values were normalized to the Ct of respective total input DNA. Relative dsODN integration due to GeCas12a2 collateral activity was reported as the fold change from vehicle, which served as a baseline for background dsODN integration.

Cas12a2 off-target activation analysis

To investigate potential alternative targets of Cas12a2, the gRNA sequence under investigation was pasted into the Cas-OFFinder online tool[74]. The PAM SpRY Cas9 from *Streptococcus pyogenes*: 5′-NNN-3′ was selected and the genome searched was 'Homo sapiens (GRCh38hg38)-Human'. As Cas12a2 targets RNA instead of DNA, the identified lower-mismatch-containing sequences were analysed using NCBI BLAST. This allowed us to identify the nucleotides surrounding the potential targeting region (including the 3′ PFS sequences), the location in the genome, and whether or not the sequence is part of an intrinsic region of DNA or an RNA transcript. To predict potential activating RNAs within the transcriptome, a cDNA search was performed using NCBI Nucleotide BLAST. The default settings were adjusted to increase the number of hits for short queries by selecting the minimum exact hit number (wordsize = 7), optimize for somewhat similar sequences and automatically adjust parameters for short input sequences. The Reference RNA sequences (refseq_rna) database was searched, filtering for the organism *Homo sapiens* (taxid:9606). The default settings were further adjusted by increasing the max target sequences to 5,000, with an expected threshold of 100, a match/mismatch score of 1,-3 and no filter or masking. To identify sequences with the most similarity to the target sequence, the MSA viewer was used to sort the hits by coverage percentage (smallest number of mismatches). To prevent any bias, no PFS restrictions were used. Instead, all potential activating RNAs were identified and reported (Supplementary Table 6).

Off-target in vitro testing

To determine the off-targets' ability to activate the DNase activity of Cas12a2, a collateral dsDNA cleavage assay was performed, as previously described in this Article. However, as magnesium concentrations have been shown to affect Cas nucleases' specificity, we lowered the magnesium concentration of the NEB 3.1 buffer to a more physiologically relevant magnesium concentration of 1 mM Mg^{2+} (100 mM NaCl, 50 mM Tris-HCl, 1 mM $MgCl_2$, 100 μg ml^{-1} BSA, pH 7.9)[75].

HeLa-GFP/-RFP co-culture cell depletion

GeCas12a2 or SuCas12a2 RNPs were electroporated to 1×10^5 cells containing HeLa-RFP cells and an excess of HeLa-GFP cells. After four days of culture incubation in 12-well plates, samples were resuspended and analysed by flow cytometry using the Sony MA900 system with 488 nm and 561 nm laser excitation. Quantification of relative GFP^+/RFP^+ cell populations excluded non-fluorescing cells as determined by gating strategy. Data were analysed using FlowJo (v.10).

Animal experiments

Fragments of patient-derived HPV16-positive HNSCC cancer xenograft specimens (HN11303) were thawed at 37 °C and transplanted subcutaneously into immunodeficient 5–7-week-old female NOG mice weighing 20.2 g ± 1.67 g. When tumours reached a volume of 1–1.5 cm^3, the model was passaged into new mice. On the day of inoculation, tissue of passage 7 was collected. For transplantation of HN11303 fragments, tissue of passage 7 was collected and sliced into 3 × 3 to 4 × 4 mm^3 pieces. These pieces were transplanted into the left flank of the anaesthetized experimental animals into a small pocket formed with scissors. From the first day onwards, tumour volumes were recorded two times per week. Animal welfare was controlled twice daily. In the treatment study, animals were randomized (n = 5 mice per group) and treatments were applied by intratumoral injections when an average tumour volume of about 150 mm^3 was reached. The mice were treated on days 1 and 7, with two administrations per day spaced 6 h apart. In each treatment, 25 µl of the LNP formulation (containing 10 µg total RNA) or 25 µl of saline solution (vehicle control) was administered directly into the tumour. In the histology study, the animals were treated with one cycle (two injections with 6 h interval) only. Tumour volumes and mice body weights were measured twice per week. Tumour volume was calculated using the formula: tumour volume = $(\text{width}^2 \times \text{length})/2$. As toxicity parameters, body weight, clinical signs, and animal behaviour were recorded for all mice twice a week. Data were not collected in a blinded manner. Mice were held in individual ventilated cages under standardized and controlled environmental conditions. Mice were housed at 24 ± 2 °C and 50 ± 10% relative humidity under an artificial 12 h light–dark cycle (lights on at 06:00 am, lights off at 6:00 pm). The experiment was terminated when the tumour size exceeded 1.5 cm^3 as an ethical endpoint. The work conducted in living mice—at the Experimental Pharmacology and Oncology—is in accordance with the German Animal Welfare Act, and the UK Coordinating Committee on Cancer Research, and all procedures were approved by local authorities (Landesamt für Gesundheit und Soziales, LaGeSo) under approval no. E0023/23.

Indel enrichment

To induce indels in the *GFP* transgene, 1×10^5 HEK293-GFP cells were electroporated with purified FLAG-tagged FnCas12a (WP_003040289) RNPs. After electroporation (48 h), cells were detached from the 24-well plate cavities and transferred to poly-D-lysin-coated 10-cm-diameter culture dishes with the addition of 1 µg ml^{-1} tetracycline. One week after electroporation, cells were detached and subjected to indel analysis. To deplete unedited cells, 1×10^5 cells were electroporated with 50 pmol purified FLAG-tagged GeCas12a2 RNPs. After electroporation (48 h), cells were detached from the 24-well plate cavities and further cultivated on poly-D-lysin-coated 10-cm-diameter culture dishes with a medium containing 1 µg ml^{-1} tetracycline. After 10–12 days, the indel analysis was performed. For the indel analysis, genomic DNA was isolated (Quick-DNA Miniprep Plus Kit, Zymo Research), and the target region spanning parts of the cytomegalovirus (CMV) promoter and the *GFP* transgene was amplified by PCR using the CMV forward primer (5′-CCATAGTAACGCCAATAGGG-3′) and the *GFP* reverse primer (5′-TGTCGGCCATGATATAGACG-3′). The resulting amplicons were subjected to Sanger sequencing followed by determination of Indel-frequency via TIDE-analysis (https://tide.nki.nl/).

Prime edit enrichment

HEK293-GFP cells were seeded in a 24-well plate 24 h before transfection. Transfections were performed while cells were approximately 80% confluent. The transfection solution consisted of 1.5 µl X-tremeGENE HP DNA transfection reagent with 375 ng of PEmax-P2A-hMLH1dn plasmid, 125 ng of pegRNA plasmid and 41.5 ng of nicking sgRNA plasmid, these last two being cloned to target the *GAPDH* locus. The transfections were performed according to the manufacturer's protocol. Samples were moved to six-well plates two days following transfection. Three days later, samples were electroporated with GeCas12a2 RNPs against the *GAPDH* target. Sample genomes were collected with DNeasy Blood and Tissue Kit (Qiagen) following manufacturer's protocol 11 days after transfection (six days after electroporation). *GAPDH* amplicons for sequencing were prepared using primers 5′-TGAGTGCTACATGGTGAGCC-3′ and 5′-TGCAAAGAAAGAGGGAGCGG-3′. Editing efficiency was evaluated using long-read PCR sequencing (GENEWIZ).

Generation of *KRAS* and Cas12a2-expressing stable cell lines

Coding sequences for WT *KRAS*, *KRAS*^{G12C} and SuCas12a2 flanked by NLSs were cloned into a pLenti vector plasmid backbone including a P2A-GFP reporter; 10 µg of each expression plasmid, 5 µg of pMDLg/pRRE, 2.5 µg of pRSV-Rev and 2.5 µg of pMD2.G viral packaging plasmids were transfected into Lenti-X 293 T cells using polyethylenimine to produce the virus. The virus was collected, concentrated using Amicon Ultra-15 Centrifugal Filter Units (Millipore, UFC910024) and then used for transduction. Concentrated virus was added to cells in media containing 10 µg ml^{-1} polybrene; plates were gently shaken every 30 min for 3 h before the medium was replaced after 24 h. Cells with high *GFP* expression were sorted using the Sony MA900 cell sorting system.

RNA-FISH probe creation and RNA-FISH quantification of *KRAS* mRNA

Custom DNA probes against *KRAS* endogenous and overexpression constructs were designed using the Biosearch Technologies Stellaris RNA FISH Probe Designer. Designed DNA oligonucleotides were labelled with ddUTP-Cy5 (1 mM in water, Jena Bioscience, NU-1619-Cy5) using a Terminal Transferase Kit (NEB, M0315S). Labelled probes were purified and the labelling efficiency was measured using ultraviolet–visible absorbance. Cells were plated on glass coverslips in twelve-well plates and incubated for 24 h under standard culture conditions. Cells were washed with 1× PBS and fixed using 4% paraformaldehyde. Fixation was quenched with 0.1 M glycine in 1× PBS and permeabilized with 0.5% Triton X-100. Cells were rinsed again with 1× PBS and denatured using 10% formamide in 2× saline-sodium citrate (SSC) buffer. The coverslips were then placed on slides containing hybridization buffer containing 200 nM of the *KRAS* probe and incubated in a dark humidified chamber at 37 °C for 3 h. Following this incubation, coverslips were transferred to a new plate and incubated with 10% formamide in 2× SSC, once at 37 °C and once at room temperature. They were rinsed a final time with 1× PBS and then mounted on a slide cell side down using ProLong Diamond Antifade Mountant with DAPI (Invitrogen). Samples were incubated at room temperature for 18–24 h, sealed and then stored at 4 °C protected from light. To quantify the amount of *KRAS* transcripts in the cells, samples were imaged using a Nikon Eclipse Ti-2 microscope alongside a CSU-W1 spinning disk confocal scanner unit (Yokogawa). The samples were excited using four laser wavelengths: 405 nm, 488 nm, 561 nm and 640 nm. The fluorescence signals were captured using a Plan Apo 60× objective (Nikon, NA 1.40) and detected using a high-speed Kinetix sCMOS camera (photometrics). All imaging data were examined, processed and quantified using Fiji, Ilastik and Cell Profiler.

Generation of sotorasib-resistant cells

Sotorasib was purchased from MedChemExpress (Monmouth Junction). To achieve cellular resistance to this molecule, three biological replicates of NCI-H23 cells were exposed to progressively higher concentrations of sotorasib for one week each (1 µM, 2.5 µM, 5 µM and finally 10 µM); the surviving cells were propagated similarly to past protocols[48].

Statistics and reproducibility

All statistical analyses and significance levels are defined in the figure legends. Exact *P* values for all comparisons are compiled in the Source data. Refer to Supplementary Fig. 1 for gel source data.

Reporting summary

Further information on research design is available in the Nature Portfolio Reporting Summary linked to this article.

Data availability

RNA-seq and PFS screening data are publicly available at NCBI GEO under accession no. GSE325194. The human Hallmark Gene Sets collection from the Molecular Signatures Database is available for public download at gsea-msigdb.org. All relevant gRNA and target sequences supporting this study are available within this Article and the Supplementary Information. Source data are provided with this paper.

59. Robert, X. & Gouet, P. Deciphering key features in protein structures with the new ENDscript server. *Nucleic Acids Res.* **42**, W320–W324 (2014).
60. Sievers, F. & Higgins, D. G. Clustal Omega, accurate alignment of very large numbers of sequences. *Methods Mol. Biol.* **1079**, 105–116 (2014).
61. Steenwyk, J. L., Buida, T. J. III, Li, Y., Shen, X.-X. & Rokas, A. ClipKIT: a multiple sequence alignment trimming software for accurate phylogenomic inference. *PLoS Biol.* **18**, e3001007 (2020).
62. Minh, B. Q. et al. IQ-TREE 2: new models and efficient methods for phylogenetic inference in the genomic era. *Mol. Biol. Evol.* **37**, 1530–1534 (2020).
63. Gietz, R. D. & Schiestl, R. H. High-efficiency yeast transformation using the LiAc/SS carrier DNA/PEG method. *Nat. Protoc.* **2**, 31–34 (2007).
64. Trothe, J. et al. Hypotonic stress response of human keratinocytes involves LRRC8A as component of volume-regulated anion channels. *Exp. Dermatol.* **27**, 1352–1360 (2018).
65. Dobin, A. et al. STAR: ultrafast universal RNA-seq aligner. *Bioinformatics* **29**, 15–21 (2013).
66. Li, B. & Dewey, C. N. RSEM: accurate transcript quantification from RNA-seq data with or without a reference genome. *BMC Bioinf.* **12**, 323 (2011).
67. Li, H. et al. The sequence alignment/map format and SAMtools. *Bioinformatics* **25**, 2078–2079 (2009).
68. Langmead, B. & Salzberg, S. L. Fast gapped-read alignment with Bowtie 2. *Nat. Methods* **9**, 357–359 (2012).
69. Love, M. I., Huber, W. & Anders, S. Moderated estimation of fold change and dispersion for RNA-seq data with DESeq2. *Genome Biol.* **15**, 550 (2014).
70. Subramanian, A. et al. Gene set enrichment analysis: a knowledge-based approach for interpreting genome-wide expression profiles. *Proc. Natl Acad. Sci. USA* **102**, 15545–15550 (2005).
71. Korotkevich, G. et al. Fast gene set enrichment analysis. Preprint at *bioRxiv* https://doi.org/10.1101/060012 (2021).
72. Liberzon, A. et al. The molecular signatures database (MSigDB) hallmark gene set collection. *Cell Syst* **1**, 417–425 (2015).
73. Malinin, N. L. et al. Defining genome-wide CRISPR-Cas genome-editing nuclease activity with GUIDE-seq. *Nat. Protoc.* **16**, 5592–5615 (2021).
74. Bae, S., Park, J. & Kim, J.-S. Cas-OFFinder: a fast and versatile algorithm that searches for potential off-target sites of Cas9 RNA-guided endonucleases. *Bioinformatics* **30**, 1473–1475 (2014).
75. Nguyen G. T. et al. CRISPR-Cas12a exhibits metal-dependent specificity switching. *Nucleic Acids Res.* https://doi.org/10.1093/nar/gkae613 (2024).
76. Scholtz, P., Zurek, C. & Krohn, M. Novel, non-naturally occurring CRISPR-Cas nucleases for genome editing. World Patent no. WO/2022/017633 (2022).

Acknowledgements We gratefully acknowledge A. Knapp, K. Przibilla, N. Schade, R. Heger and J. Noske for their technical assistance. We thank A. Lyons, L. Ostertag and R. Peterson for preliminary efforts to demonstrate cell targeting with SuCas12a2. We thank R. Vawdrey and I. Pantziris for their creation of the plasmids and cell lines used for cell elimination. pCMV-PEmax-P2A-hMLH1dn and pU6-pegRNA-GG-acceptor were gifts from D. Liu. pSPgRNA was a gift from C. Gersbach. pBabe-KRAS Wt and pBabe-KRAS G12C were gifts from C. Der. Research reported in this publication used the High-Throughput Genomics and Cancer Bioinformatics Shared Resource at the Huntsman Cancer Institute at the University of Utah, and was supported by the National Cancer Institute of the National Institutes of Health (award no. P30CA042014). We also acknowledge J. Johnson, and the HSC Cell Imaging and Flow Cytometry Cores at the University of Utah for allowing use of their equipment. Funding was provided via the R. Gaurth Hansen Family (to R.N.J.), the National Institutes of Health (grant nos. R35GM138080 to R.N.J., R35GM150941 to Y.L. and T32GM141848 to G.S.) and the European Research Council (grant no. 101158249 to C.L.B.).

Author contributions P.S., J.T., M.K., R.N.J., C.L.B. and Y.L conceptualized the work. J.T. (SuCas12a2), T.F. and P.S. (GeCas12a2) performed the original demonstration of mammalian cell killing. J.T., K.T.C., T.F., N.M.K., G.S., R.B., Z.A.B., A.J., C.Z., O.D., F.S., E.W. and X.Z designed

the methodology. J.T., K.T.C., F.S. and O.D did the in vitro and bacterial work; C.Z. and T.F worked on the yeast cells; and P.S., J.T., T.F., N.M.K., G.S., R.B., Z.A.B., A.J. and Y.L worked on the mammalian cells. K.T.C., T.F., R.B. and C.Z prepared the RNPs. J.T., K.T.C. and A.J. predicted and analysed the off-target activation. J.T., O.D., E.W. and X.Z performed RNA sequencing and NGS analysis. D.S., R.M. and P.S designed the in vivo study and interpreted the data. P.S., M.K., J.R., X.Z., R.N.J., C.L.B. and Y.L supervised the work. J.T., K.T.C., R.N.J., C.L.B. and Y.L wrote the original draft, which was reviewed and edited by all authors. P.S., M.K., R.N.J., C.L.B. and Y.L acquired funding.

Competing interests BRAIN Biotech AG has filed patent applications that cover the GeCas12a2 nuclease sequence (WO 2022/017633) and its use for cell depletion (WO 2023/139096), with P.S., C.Z. and M.K. as inventors. The Helmholtz Centre for Infection Research and Utah State University have filed provisional patent applications on Cas12a2 and its applications (WO 2022/253903A1), with O.D., R.N.J. and C.L.B. as inventors. C.L.B. is a co-founder and scientific advisor to Locus Biosciences, a co-founder and officer of Leopard Biosciences GmbH, and scientific advisor to Benson Hill. C.Z. is an employee of BRAIN Biotech. A.G., P.S., T.F., R.B., D.S. and R.M. are employees of Akribion Therapeutics GmbH. M.K. is a co-founder and co-CEO of Akribion Therapeutics GmbH. The remaining authors declare no competing interests.

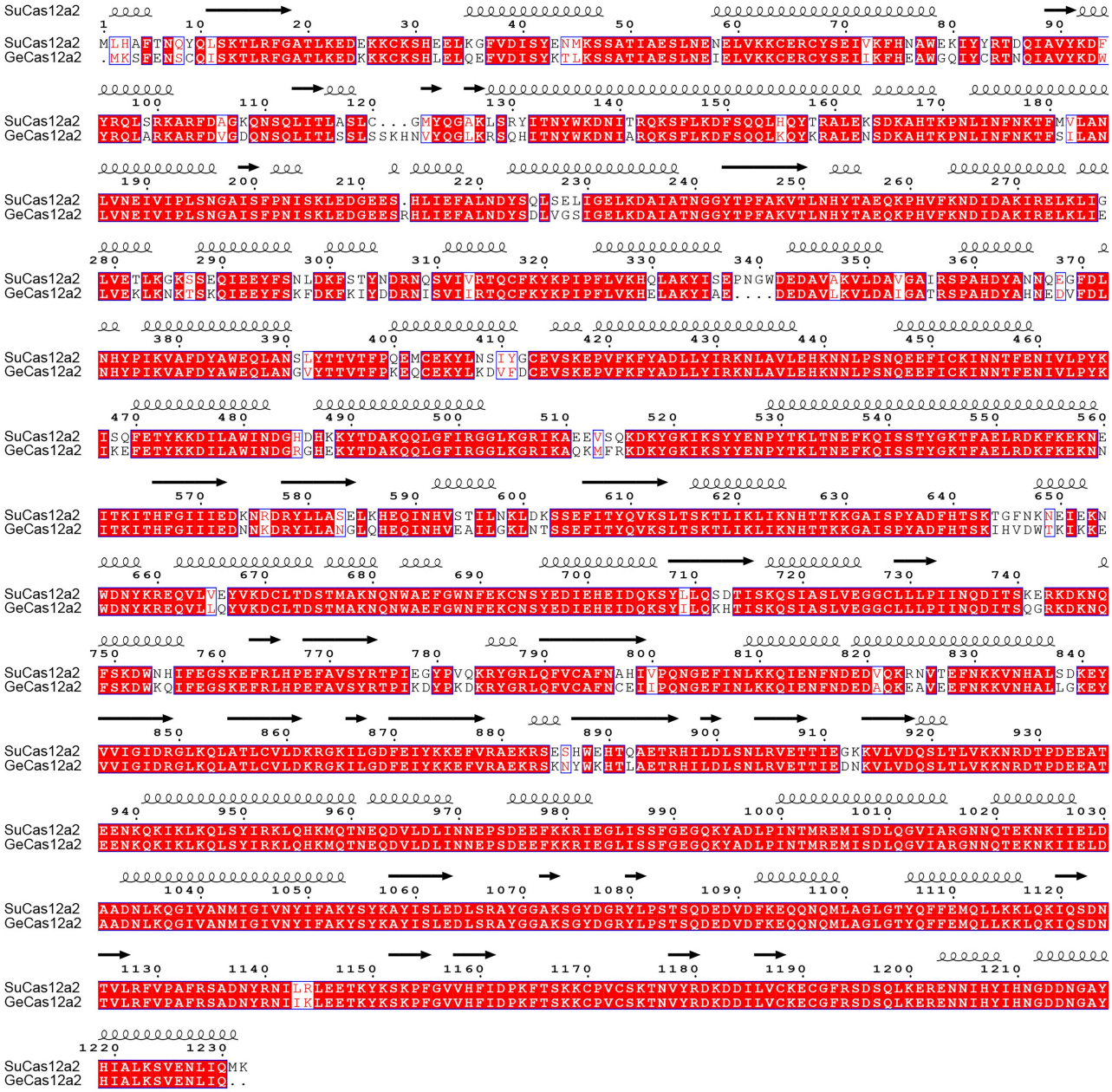
Additional information

Supplementary information The online version contains supplementary material available at https://doi.org/10.1038/s41586-026-10466-y.

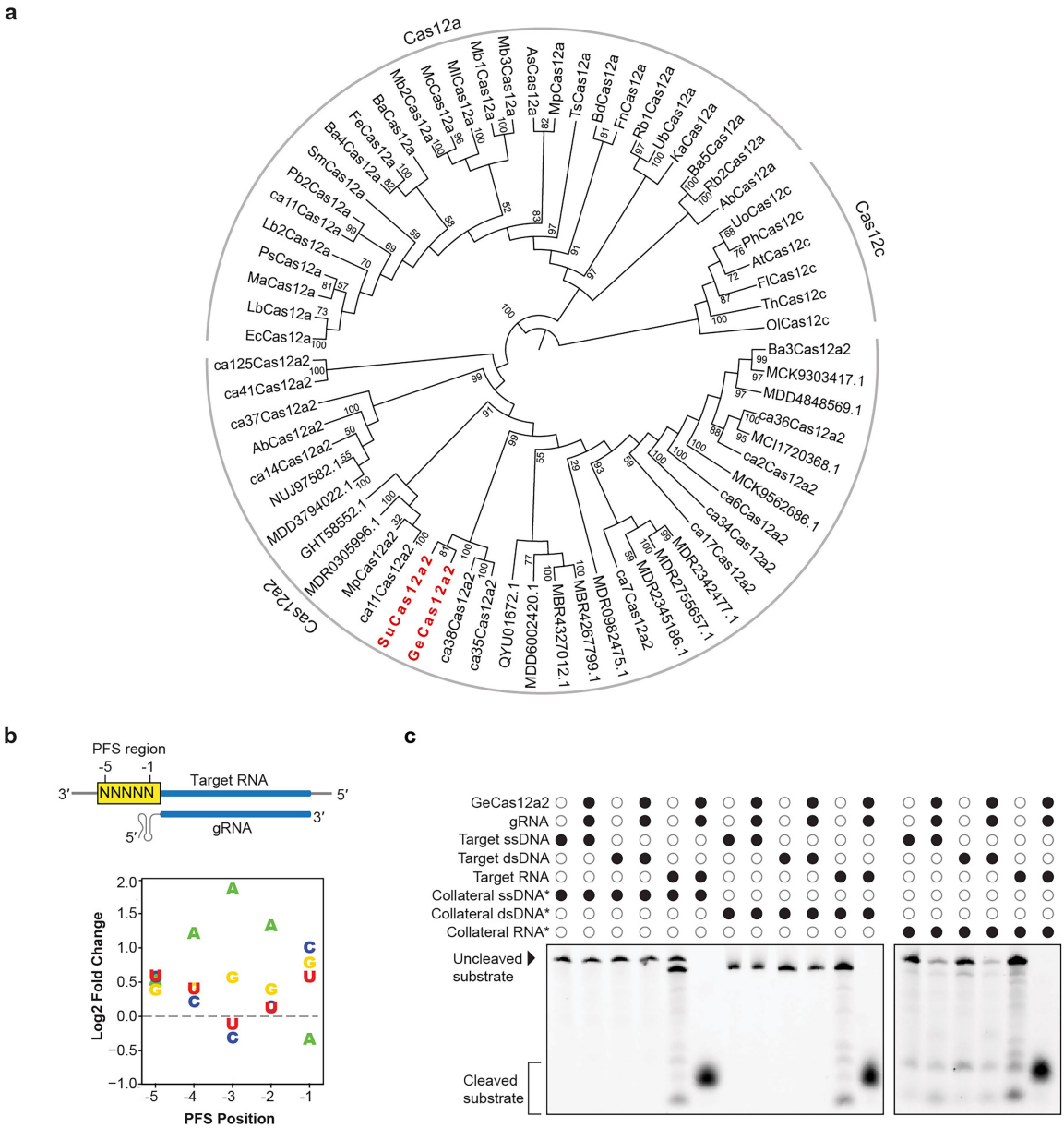
Correspondence and requests for materials should be addressed to Paul Scholz, Ryan N. Jackson, Chase L. Beisel or Yang Liu.

Peer review information *Nature* thanks Raymond Staals, who co-reviewed with Mehran Takallo, and the other, anonymous, reviewer(s) for their contribution to the peer review of this work.

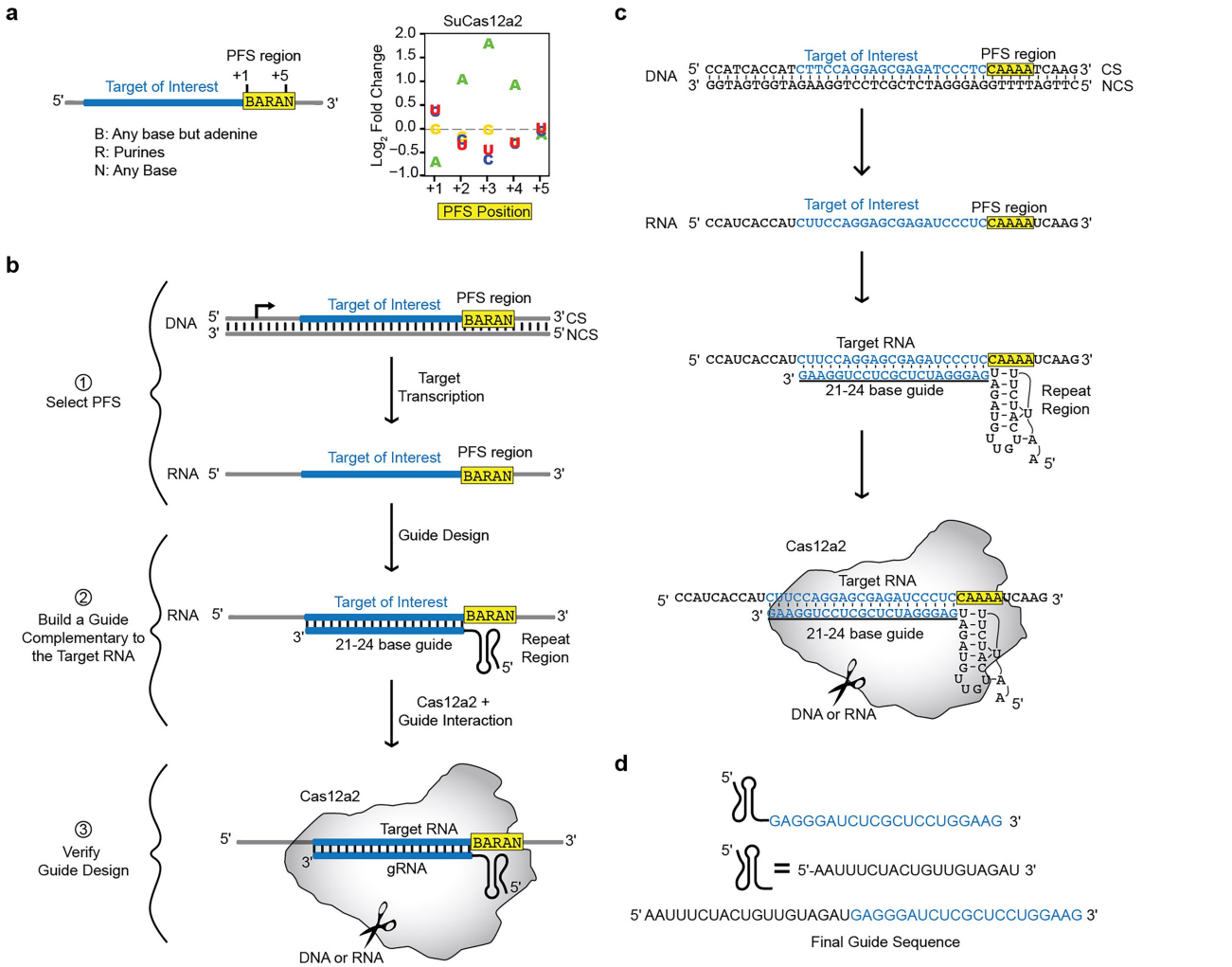
Reprints and permissions information is available at http://www.nature.com/reprints.



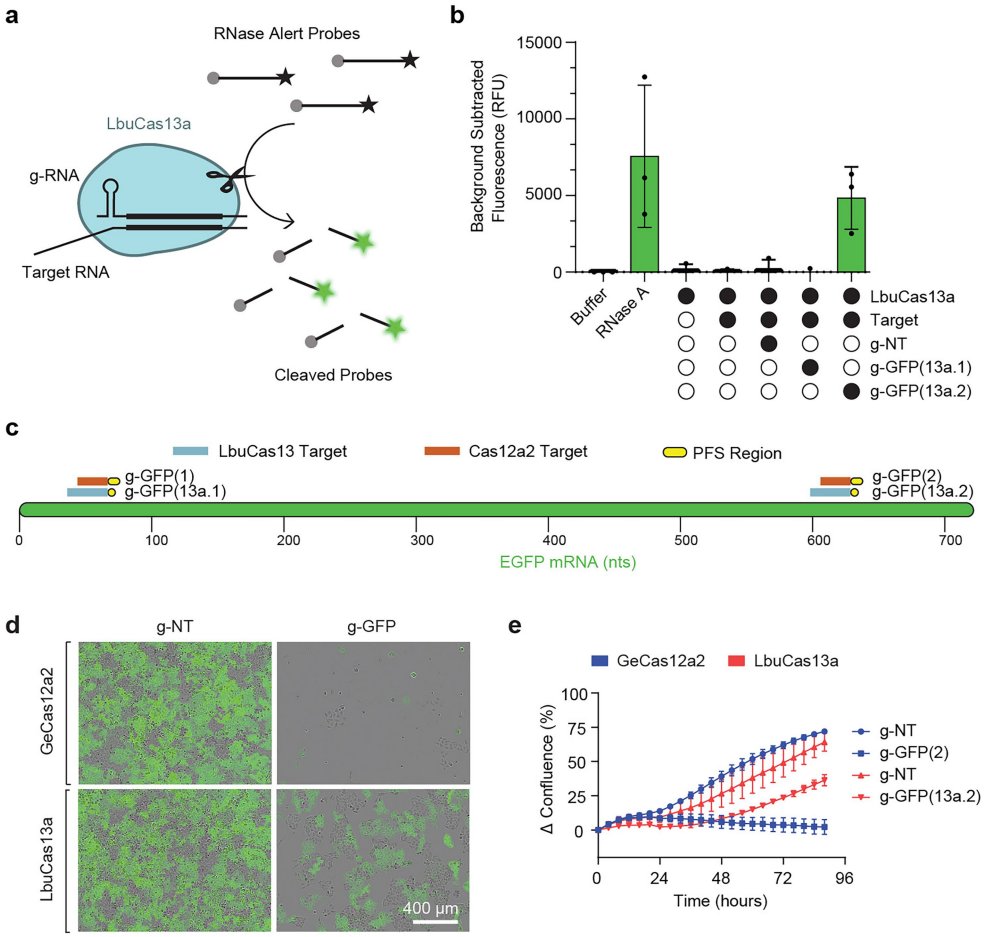
Extended Data Fig. 1 | GeCas12a2 and SuCas12a2 are similar in sequence. Amino acid sequence alignment of SuCas12a2 and GeCas12a2. Above the alignment shows the Cryo-EM solved secondary structure of SuCas12a2 (PDB: 8D4A) with beta sheets represented as arrows and alpha helices represented as coils[59].



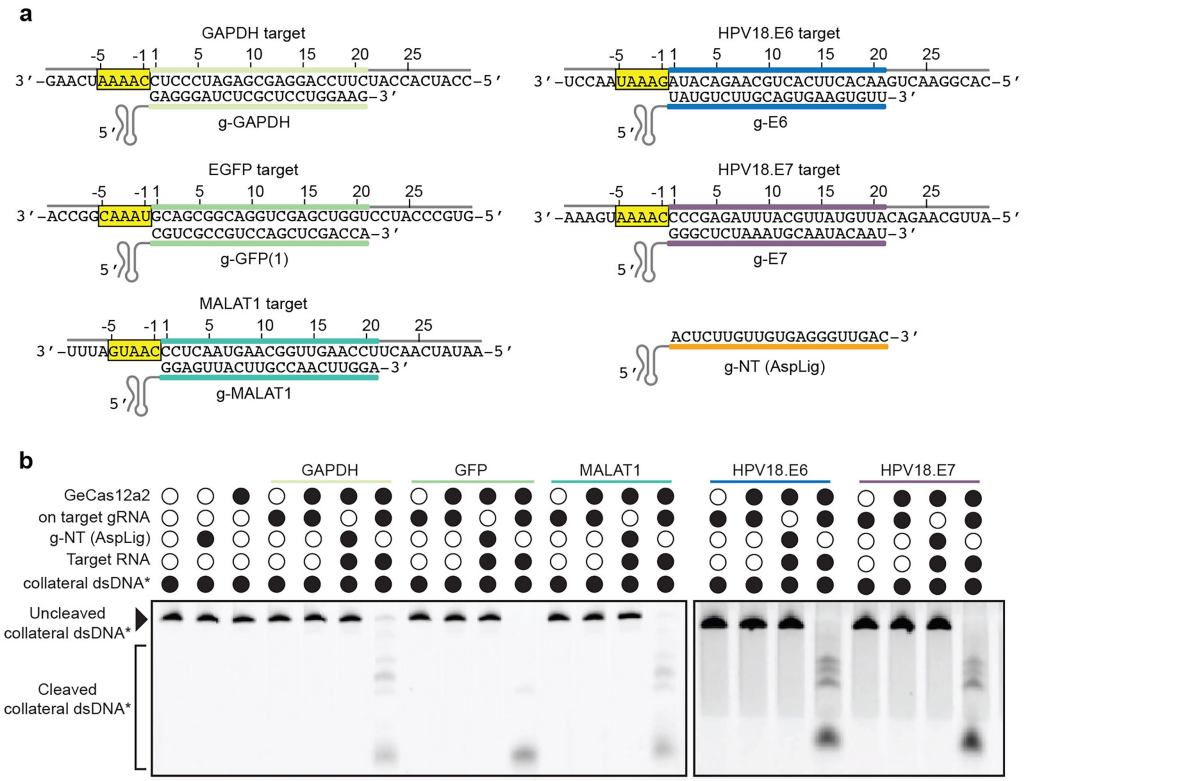
Extended Data Fig. 2 | GeCas12a2 and SuCas12a2 are similar in activation requirements (RNA target and similar PFS), and collateral cleavage substrates. a) Dendrogram displaying Cas12 nucleases with Cas12c being the outgroup. Highlighted in red are GeCas12a2 and SuCas12a2. Branch confidence is shown on a 1-100 scale as ultrafast bootstrap values (UFBoot)[76]. **b**) PFS sequence depletion assay results for GeCas12a2. Results are representative of duplicate independent experiments starting from separate colonies. **c**) In vitro collateral cleavage results are representative of three independent replicates, asterisks represent the fluorescently labelled substrates that are visualized for fluorescein fluorescence after being run on a denaturing UREA-PAGE gel. For gel source data, see Supplementary Fig. 1.



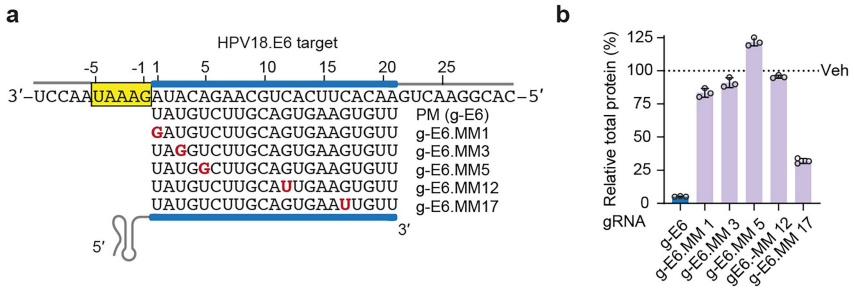
Extended Data Fig. 3 | Cas12a2 guide design parameters. a) Schematic of Cas12a2's target RNA with the preferred PFS sequence of SuCas12a2 (left), according to the previously published PFS depletion assay results (right)[15]. **b**) Steps taken to design a Cas12a2 guide RNA to target RNA, starting from either a DNA or RNA target sequence. The pair of scissors represents Cas12a2's RuvC active site. **c**) Shows an example of how the guide RNA targeting the *GAPDH* transcript was designed. **d**) The final guide RNA sequence, including the repeat region (black) and the targeting region (blue).



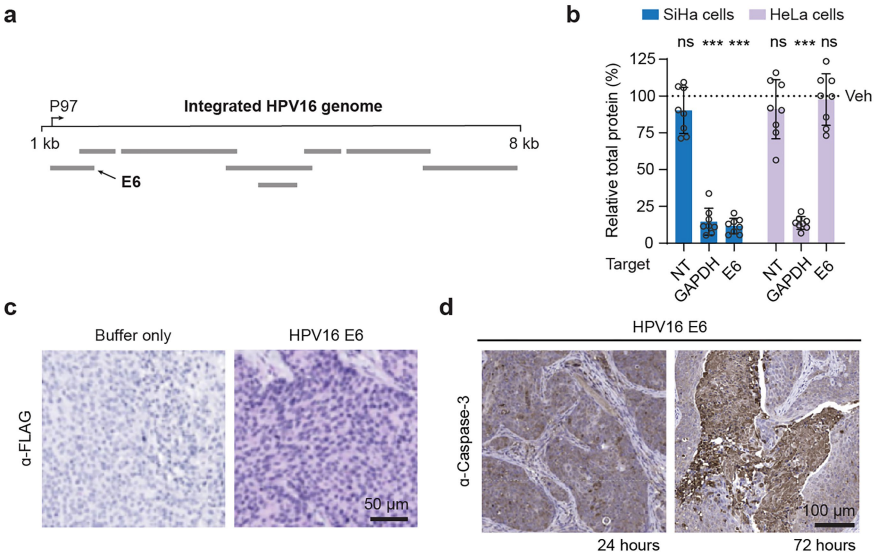
Extended Data Fig. 4 | Comparison of GeCas12a2 and LbuCas13a cell-killing activity. a) Detection of activation and collateral nuclease activity of LbuCas13a using fluorescently labelled RNA substrate in vitro. **b**) Quantification of LbuCas13a activation in vitro by fluorescence signal under a non-targeting condition (g-NT) or two *GFP*-targeting conditions (g-GFP(13a.1), g-GFP(13a.2)). **c**) Tested LbuCas13a gRNAs encompass target sites for known Cas12a2 gRNAs. **d**) Overlaid phase contrast and GFP fluorescence microscopy images following electroporation with either GeCas12a2 or LbuCas13a against the indicated targets in HeLa-GFP cells. **e**) Growth curves over time by phase imaging (confluence) following electroporation with either GeCas12a2 or LbuCas13a against the indicated targets. Growth curves represent the average of three biological replicates. Circles in **b** represent biological replicates (n = 3), bars and error bars represent the mean and s.d.



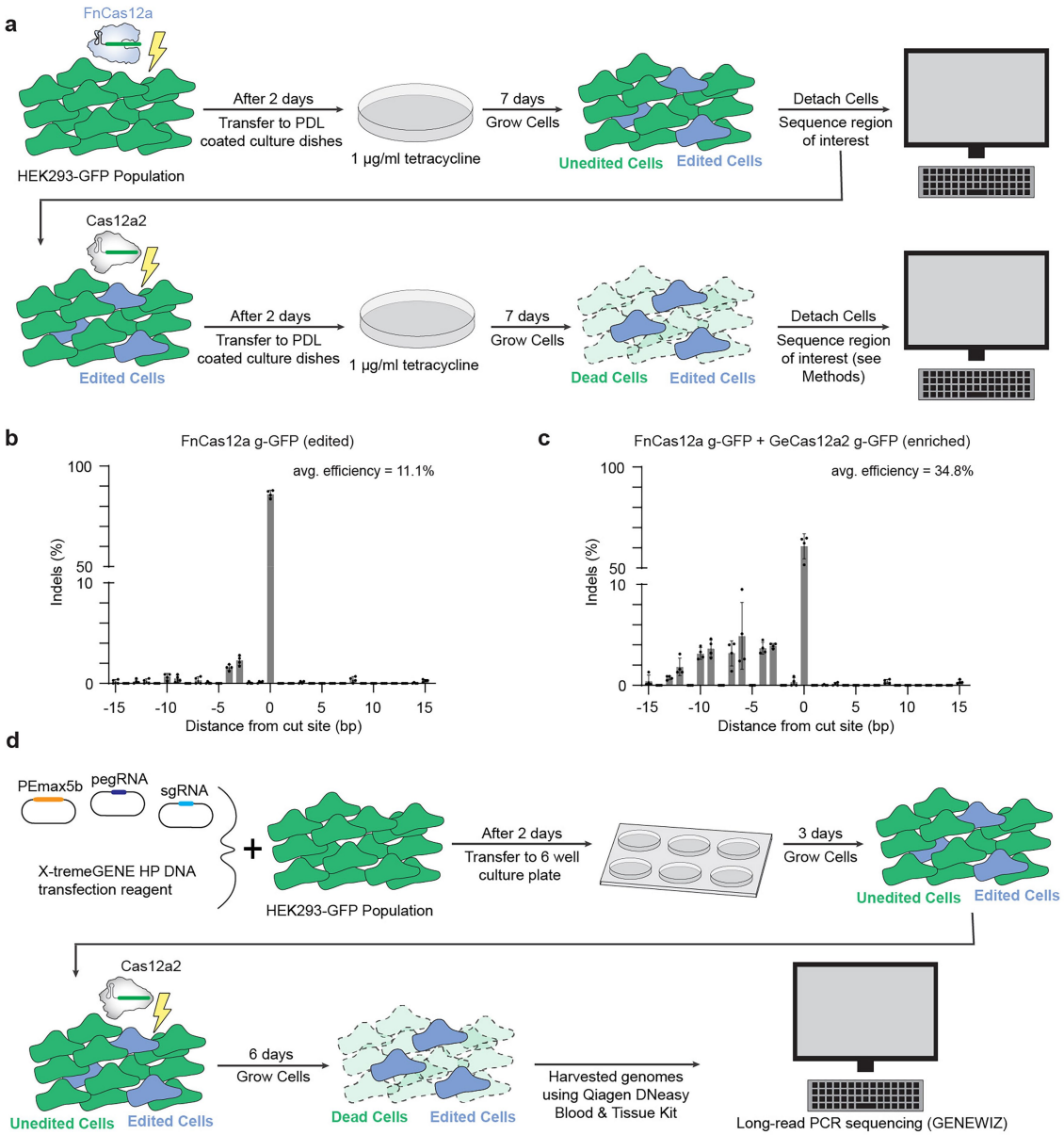
Extended Data Fig. 5 | Cas12a2 collaterally degrades dsDNA when targeting endogenous transcripts in vitro. a) Schematic of target RNAs with Protospacer Flanking Sequences (PFS) highlighted in yellow and each of the endogenous guide RNAs used in vitro and in HeLa-GFP cells. The sequence of the grey 5′ hairpin of the guides is 5′-AAUUUCUACUGUUGUAGAU-3′. **b**) In vitro collateral dsDNA cleavage assay using GeCas12a2. The asterisks represent the fluorescently labelled dsDNA collateral substrate, which is visualized for fluorescein fluorescence after being run on a denaturing UREA-PAGE gel. The gels are representative of three technical replicates. For gel source data, see Supplementary Fig. 1.



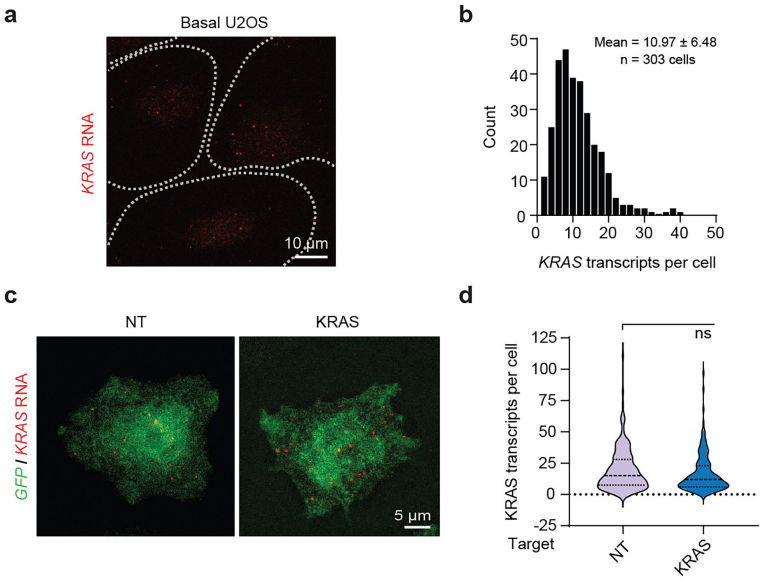
Extended Data Fig. 6 | Cas12a2 exhibits specificity for single-nucleotide mismatches. a) Assessing the impact of select single-nucleotide gRNA mismatches against the HPV18.E6 target. **b**) Cell quantification by SRB following electroporation of GeCas12a2 RNPs with the indicated mismatched gRNAs in HeLa-GFP cells, normalized to vehicle. Circles in **b** represent biological replicates (n = 3), bars and error bars represent the mean and s.d.



Extended Data Fig. 7 | GeCas12a2 selectively removes HPV-harbouring cells, is stably expressed, and triggers apoptosis in vivo. a) Targeting within the *E6* transcript of HPV16. **b**) Cell quantification by SRB following electroporation with GeCas12a2 against the indicated targets in HPV16-positive SiHa cells or HeLa cells, normalized to vehicle. **c**) FLAG stains from one tumour cryosection 24 h post-injection showing expression of the FLAG-tagged GeCas12a2 nuclease following administration of the active formulation. **d**) Tumour cryosections from one tumour after 24 and 72 h post-injection showing delayed Caspase-3 expression, consistent with in vitro experiments. Circles in **b** represent biological replicates (n = 8), bars and error bars represent the mean and s.d. Two-tailed unpaired t-test with Welch's correction was performed, ns: $p > 0.05$. ***: $p < 0.001$.



Extended Data Fig. 8 | Cas12a2 enables enrichment of gene-edited cells. **a**) Experimental workflow for generating indels in heterologous *GFP* loci with FnCas12a followed by counterselection of cells lacking indels with GeCas12a2. **b**,**c**) Quantification of indel distributions by Sanger sequencing TIDE analysis following electroporation with (**b**) on-target FnCas12a and non-target GeCas12a RNPs or (**c**) on-target FnCas12a and on-target GeCas12a2 RNPs against their respective *GFP* targets. **d**) Experimental workflow for generating prime edits in endogenous *GAPDH* loci with PEmax5 or PEmax5b followed by counterselection of cells lacking prime edits with GeCas12a2. Circles in **b** and **c** represent biological replicates (n = 4), bars and error bars represent the mean and s.d.



Extended Data Fig. 9 | KRAS transcription levels in basal U2OS and post-RNP electroporated NCI-H23-GFP cells. a) Confocal image of endogenously expressed WT *KRAS* transcripts (red) in U2OS cells. Representative of three biological replicates. **b**) Histogram of WT *KRAS* transcript copy number per U2OS cell. Histogram includes all cells analysed from three biological replicates (n = 303 cells). **c**) Confocal images of endogenously expressed *KRAS* transcripts (red) following electroporation with GeCas12a2 RNPs against the indicated target transcripts and survivor outgrowth in NCI-H23-GFP cells (green). Representative of three biological replicates. **d**) Quantification of endogenous *KRAS* transcripts by RNA FISH following electroporation of GeCas12a2 RNPs against the indicated targets and survivor outgrowth in NCI-H23-GFP cells. Violin plot includes all cells analysed from three biological replicates (n = 189 cells for NT, 153 cells for KRAS). Dashed lines represent relative quartiles. Two-tailed unpaired t-test with Welch's correction was performed, ns: $p > 0.05$.

nature portfolio

Corresponding author(s): Yang Liu, Paul Scholz, Chase Beisel, Ryan Jackson

Last updated by author(s): Mar 17, 2026

Reporting Summary

Nature Portfolio wishes to improve the reproducibility of the work that we publish. This form provides structure for consistency and transparency in reporting. For further information on Nature Portfolio policies, see our Editorial Policies and the Editorial Policy Checklist.

Statistics

For all statistical analyses, confirm that the following items are present in the figure legend, table legend, main text, or Methods section.

n/a	Confirmed
☐	☒ The exact sample size (*n*) for each experimental group/condition, given as a discrete number and unit of measurement
☐	☒ A statement on whether measurements were taken from distinct samples or whether the same sample was measured repeatedly
☐	☒ The statistical test(s) used AND whether they are one- or two-sided *Only common tests should be described solely by name; describe more complex techniques in the Methods section.*
☒	☐ A description of all covariates tested
☐	☒ A description of any assumptions or corrections, such as tests of normality and adjustment for multiple comparisons
☐	☒ A full description of the statistical parameters including central tendency (e.g. means) or other basic estimates (e.g. regression coefficient) AND variation (e.g. standard deviation) or associated estimates of uncertainty (e.g. confidence intervals)
☐	☒ For null hypothesis testing, the test statistic (e.g. *F*, *t*, *r*) with confidence intervals, effect sizes, degrees of freedom and *P* value noted *Give P values as exact values whenever suitable.*
☒	☐ For Bayesian analysis, information on the choice of priors and Markov chain Monte Carlo settings
☒	☐ For hierarchical and complex designs, identification of the appropriate level for tests and full reporting of outcomes
☒	☐ Estimates of effect sizes (e.g. Cohen's *d*, Pearson's *r*), indicating how they were calculated

Our web collection on statistics for biologists contains articles on many of the points above.

Software and code

Policy information about availability of computer code

Data collection

1. Cell depletion measurement via SRB assay was performed using FlexStation 3 (Molecular Devices) or Biotek Synergy Neo2 (Agilent) microplate readers and accompanying softwares.
2. Cell depletion measurement via phase confluence, cell counting, and GFP intensity was performed using the Incucyte® SX5 system (Sartorius) and Incucyte® Base Analysis Software (v2023A).
3. DNA damage foci and RNA FISH imaging was carried out using an Eclipse Ti-2 spinning disk confocal microscope (Nikon) equipped with Nikon NIS-Elements software (v6.02.03).
4. Flow cytometry was conducted using FACSCelesta (BD Biosciences) or MA900 (Sony) and accompanying softwares.
5. RNA-seq was perfomed using Hiseq 4000 (Illumina) or NovaSeq X series (Illumina).
6. qPCR was performed using QuantStudio 3 (ThermoFisher) and accompanying software.

Data analysis

1. Incucyte's standard basic analysis (AI confluence, GFP count per image, Total integrated intensity) and adherent cell-by-cell analysis (Phase object count per image) were used to quantify cell depletion over time and at endpoints.
2. Fiji ImageJ v2 was used to reduce background noise in the fluorescence images of DNA damage foci.
3. Ilastik v1 and built-in modules were used to segment cell bodies in fluorescence images of RNA FISH.
4. CellProfiler v4 and built-in modules were employed to automatically segment and quantify cell nuclei, DNA damage foci, and RNA FISH transcripts.
5. FlowJo v10.10 was utilized to gate and analyze flow cytometry data.
6. RStudio v4 was used to execute differential gene expression analysis and hallmark pathway. Sequencing reads were aligned to hg38 with Bowtie2 (v2.2.9). Read counts for each GENCODE gene were quantified with RSEM (v1.2.28). DESeq2 (v1.44.0) was used to normalize the read counts and perform differential expression analysis. Gene set enrichment analysis (GSEA v4.3.3) was run to determine the enriched gene sets.

The R package fgsea (v1.30.0) was used to calculate the normalized enrichment statistics for each gene set in the Hallmark Collection from the Molecular Signatures Database (PMID: 26771021).

For manuscripts utilizing custom algorithms or software that are central to the research but not yet described in published literature, software must be made available to editors and reviewers. We strongly encourage code deposition in a community repository (e.g. GitHub). See the Nature Portfolio guidelines for submitting code & software for further information.

Data

Policy information about availability of data

All manuscripts must include a data availability statement. This statement should provide the following information, where applicable:

- Accession codes, unique identifiers, or web links for publicly available datasets
- A description of any restrictions on data availability
- For clinical datasets or third party data, please ensure that the statement adheres to our policy

All relevant sequencing data are publicly available at NCBI GEO under accession number GSE287139. The human Hallmark Gene Sets collection from the Molecular Signatures Database is available for public download at gsea-msigdb.org. All relevant gRNA and target sequences supporting this study are available within this article and the Supplementary Information section.

Research involving human participants, their data, or biological material

Policy information about studies with human participants or human data. See also policy information about sex, gender (identity/presentation), and sexual orientation and race, ethnicity and racism.

Reporting on sex and gender	N/A
Reporting on race, ethnicity, or other socially relevant groupings	N/A
Population characteristics	N/A
Recruitment	N/A
Ethics oversight	N/A

Note that full information on the approval of the study protocol must also be provided in the manuscript.

Field-specific reporting

Please select the one below that is the best fit for your research. If you are not sure, read the appropriate sections before making your selection.

☒ Life sciences ☐ Behavioural & social sciences ☐ Ecological, evolutionary & environmental sciences

For a reference copy of the document with all sections, see nature.com/documents/nr-reporting-summary-flat.pdf

Life sciences study design

All studies must disclose on these points even when the disclosure is negative.

Sample size	For cell imaging of 53BP1 foci, samples sizes were chosen to meet or exceed those of existing publications with similar analyses (PMIDs: 31645724; 32527834; 37024653). For all other studies, we conducted at least three biological replicates as the minimum number of independent replicates necessary to calculate standard deviation, perform statistical comparisons, and ensure reproducibility.
Data exclusions	During flow cytomtery analysis of GFP and RFP positive cells within a co-culture, cells which were gated as negative for either fluorescent reporter were excluded from quantification of total events. This exclusion criterion was pre-established given that negative cells contain neither the on-target nor off-target transcript necessary for analysis of Cas12a2 nuclease activation, and therefore represent sample impurities. This exclusion does not change the qualitative conclusion drawn from the dataset.
Replication	In vivo experiments were performed with five animals per treatment group. All cell assays were performed with three to eight biological replicates. In vitro cleavage assays were performed with three independent replicates, although only one representative gel image is shown. All attempts at replication were successful.
Randomization	For all cell-based experiments, cells were randomly allocated from growth cultures into experimental groups. All growth cultures were maintained under identical environmental conditions (save respective media) to mitigate covariates. For instrument-based assays, cells from experimental groups were randomly sampled to counter instrument measurement bias. Mice were randomized into experimental groups to counter possible selection bias. Randomization was not required for in vitro biochemical assays due to the lack of biological covariates.
Blinding	Data were not collected in a blinded manner. However, we applied the same analysis pipelines and gating strategies to all control and experimental samples. For instance, to measure average fluorescent 53BP1 foci in given cell populations, we used DAPI signal to segment all

cell nuclei in the field of view and quantified 53BP1 foci in those nuclei.

Reporting for specific materials, systems and methods

We require information from authors about some types of materials, experimental systems and methods used in many studies. Here, indicate whether each material, system or method listed is relevant to your study. If you are not sure if a list item applies to your research, read the appropriate section before selecting a response.

Materials & experimental systems

n/a	Involved in the study
☐	☒ Antibodies
☐	☒ Eukaryotic cell lines
☒	☐ Palaeontology and archaeology
☐	☒ Animals and other organisms
☒	☐ Clinical data
☒	☐ Dual use research of concern
☒	☐ Plants

Methods

n/a	Involved in the study
☒	☐ ChIP-seq
☐	☒ Flow cytometry
☒	☐ MRI-based neuroimaging

Antibodies

Antibodies used

All antibodies are commercially available and validated.

For DNA damage foci imaging:
1. Rabbit anti-53BP1 antibody (Novus Biologicals, NB100-306)
2. Goat anti-Rabbit Alexa Fluor Plus 647 secondary antibody (Invitrogen, A32733)

For apoptosis analysis:
3. Alexa Fluor 647 Annexin-V antibody (BD Pharmingen, 567356)

Validation

1. https://www.bio-techne.com/p/antibodies/53bp1-antibody_nb100-305
2. https://www.thermofisher.com/antibody/product/Goat-anti-Rabbit-IgG-H-L-Highly-Cross-Adsorbed-Secondary-Antibody-Polyclonal/A32733
3. https://www.bdbiosciences.com/en-us/products/reagents/flow-cytometry-reagents/research-reagents/single-color-antibodies-ruo/alexa-fluor-647-annexin-v.567356?tab=product_details

Eukaryotic cell lines

Policy information about cell lines and Sex and Gender in Research

Cell line source(s)

We included a detailed Table S11 in the Supplementary Information, describing all yeast and bacterial strains, as well as the mammalian cell lines used in this study, along with their sources.

Authentication

We primarily used commercially sourced cell lines and therefore did not perform independent authentication. However, we performed RNA-seq to verify the expression levels of our RNA targets, and these data are detailed in Table S2.

Mycoplasma contamination

All cultured mammalian cell lines were tested monthly for mycoplasma contamination using the PlasmoTest kit (InvivoGen, rep-pt1), and were consistently negative.

Commonly misidentified lines
(See ICLAC register)

No commonly misidentified lines were used.

Animals and other research organisms

Policy information about studies involving animals; ARRIVE guidelines recommended for reporting animal research, and Sex and Gender in Research

Laboratory animals

5-7 weeks old NOG mice weighing 20.2 g ± 1.67 g were used for this study

Wild animals

No wild animals were used for this study.

Reporting on sex

Immunodeficient female NOG mice were used for this study.

Field-collected samples

The study did not involve samples collected from the field.

Ethics oversight

The work conducted in living mice, at Experimental Pharmacology and Oncology GmbH (Berlin, Germany), is in accordance with the German Animal Welfare Act as well as the UKCCCR (United Kingdom Coordinating Committee on Cancer Research) and all

procedures were approved by local authorities (Landesamt für Gesundheit und Soziales, LaGeSo Berlin, Germany) under approval number E0023/23.

Note that full information on the approval of the study protocol must also be provided in the manuscript.

Plants

Seed stocks	N/A
Novel plant genotypes	N/A
Authentication	N/A

Flow Cytometry

Plots

Confirm that:

☒ The axis labels state the marker and fluorochrome used (e.g. CD4-FITC).

☒ The axis scales are clearly visible. Include numbers along axes only for bottom left plot of group (a 'group' is an analysis of identical markers).

☒ All plots are contour plots with outliers or pseudocolor plots.

☒ A numerical value for number of cells or percentage (with statistics) is provided.

Methodology

Sample preparation	For apoptosis analysis: 48 hours post electroporation, cells were treated with 0.05% Trypsin, centrifuged, and resuspended in Annexin-V binding buffer (10 mM HEPES, 140 mM NaCl, 2.5 mM CaCl2, pH 7.4). Resuspended cells were mixed with Alexa Fluor 647 Annexin-V antibody (BD Pharmingen, 567356) at a volumetric ratio of 1:40 and incubated at room temperature for 15-30 minutes. Immediately preceding data acquisition, samples were mixed with 10 µg/mL DAPI stain (BD Pharmingen, 564907) at a volumetric ratio of 1:80. For Caspase-3/7 analysis, resuspended cells were mixed with 0.2 mM NucView 405 Caspase-3/7 Substrate (Biotium, 10407) at a volumetric ratio of 1:200 and incubated for 30 minutes at room temperature. For cell cycle analysis: 48 hours post electroporation, cells were treated with 0.05% Trypsin, centrifuged, and resuspended in 200 µL phenol red-free Leibovitz's L-15 Medium followed by 200 µL of 4% PFA fixative and incubated on ice for 25 minutes. To remove fixative, cells were pelleted by centrifugation at 250 RCF for 5 minutes and washed with 500 µL L-15 twice. To stain genomic DNA, cells were pelleted again and resuspended in 500 µL of a 1x PBS solution with 10 µg/mL DAPI stain (BD Pharmingen, 564907) and 0.1% Triton-X for 15 minutes at room temperature followed by 10 minutes on ice. Cells were strained through a 35 µm mesh cap before analysis to ensure single cell suspension. For co-culture depletion analysis: Four days post electroporation, HeLa-GFP and HeLa-RFP cell co-cultures were treated with 0.05% Trypsin, centrifuged, and resuspended in 400 uL phenol red-free Leibovitz's L15 Medium and analyzed by flow cytometry using the Sony MA900 system with 488 nm and 561 nm laser excitation.
Instrument	BD FACSCelesta or Sony MA900
Software	FlowJo V10.10
Cell population abundance	10,000 events per condition/sample
Gating strategy	Viable and dying single cells were gated using SSC area versus FSC area (SSC-A x FSC-A). For assessment of fluorescent apoptosis markers, cells were gated using DAPI area versus Alexa Fluor 647 Annexin-V area (BV421-A x APC-A; “Annexin-V”) or cell count versus NucView 405 area (Count x BV421-A, “Caspase-3/7”). Boundaries separating positive from negative cell populations were set between 10^2 and 10^3 arbitrary intensities. For discrimination between GFP-positive and RFP-positive cell populations, cells were gated using RFP area versus GFP area (mCherry-A x EGFP-A). Boundaries separating positive from negative cell populations were set between 10^2 and 10^3 arbitrary intensities. Cells marked as double negatives (population impurities) were excluded from quantification of total events. For cell cycle assessment, cells were gated using cell count versus DAPI area (Count x BV421-A).

☒ Tick this box to confirm that a figure exemplifying the gating strategy is provided in the Supplementary Information.